Eidgenössische Technische Hochschule Zürich
Swiss Federal Institute of Technology Zurich

Cemsuisse research project 202204

Final report

New conceptual approach to ensure the durability of reinforced concrete in XC exposure

Authors:
Thilo Schmid
Cristhiana Albert
Dr. Zhidong Zhang
Prof. Dr. Ueli Angst

Zürich, 12. December 2025

Abstract

Reducing clinker content in cement is essential for lowering CO_2 emissions but typically increases carbonation susceptibility, potentially raising corrosion risk in reinforced concrete exposed to XC environments. This project proposes a durability concept that shifts the emphasis from carbonation resistance to the moisture state of the carbonated concrete cover, recognizing moisture availability as the primary driver of corrosion propagation. Eight mortar mixes with varying binder types (CEM I, CEM II B-LL, CEM II B-M (T-LL), CEM III B) and water–binder ratios (0.5 and 0.6) were investigated. The experiments performed include monitoring electrical mortar impedance, steel potential and steel corrosion rate during wet-dry cycles, as well as the determination of moisture sorption isotherms and capillary absorption (sorptivity) tests. A two-phase moisture transport model was calibrated with experimental data and simulated moisture distribution under wet-dry cycles.

Results show that corrosion activity is negligible when the concrete remains sufficiently dry, independent of cement type. Moisture ingress consistently triggered reductions in mortar resistivity and corrosion potential, often followed by sharp increases in corrosion rate once moisture reached the steel. Sorptivity and permeability were strongly dependent on binder composition and w/b ratio, with CEM I and CEM II B-M (T-LL) exhibiting lower water ingress rates than CEM III B and CEM II B-LL mixes. Impedance measurements proved to be an early indicator of the approaching moisture front, whereas steel potential and corrosion rate provided local confirmation of moisture reaching the steel. Numerical modelling found discrepancies between mass-based and impedance-based calibration of the model parameters, highlighting the sensitivity of electrical measurements to partial saturation.

The results affirm that moisture transport (sorptivity testing) is a promising durability performance indicator for carbonated concretes. While threshold criteria cannot yet be defined, the combined experimental and modelling framework establishes a solid foundation for future standardization of moisture-based durability assessment for low-clinker concrete in XC exposure classes. Recommendations for further research are made.

Table of contents

1 Introduction

The production of Portland cement clinker causes significant greenhouse gas (GHG) emissions, with the cement and concrete industry being responsible for about 8% of global CO_2 emissions [1]. Thus, both industry and academia are seeking ways to lower these emissions by replacing part of the clinker with alternative cementitious materials. It is well known that concretes with low-emission binders are generally more prone to carbonation than conventional ordinary Portland cement (OPC) concretes. The reduction in pH caused by carbonation can, in turn, increase the risk of steel corrosion in reinforced concrete by destabilizing the passive film present on steel in alkaline environments.

For this reason, European and Swiss standards define the exposure classes XC, which prescribe durability design parameters – such as a minimum concrete cover and a sufficient carbonation resistance of the concrete – aimed at preventing carbonation and potential corrosion damage. This approach aims to ensure that carbonation, which starts at the concrete's exterior and progresses inward over time, does not reach the reinforcement during the structure's intended service life. However, current standards are conservative and tend to treat different cement types unevenly. Cements with reduced clinker contents are often penalized because they carbonate more quickly than OPC. It is therefore essential to broaden the current durability concept to a more holistic approach, which also considers the propagation phase of corrosion, after concrete has carbonated at the reinforcement level.

Both laboratory and field experiments have shown that moisture in steel reinforced concrete is the decisive factor determining whether steel corrosion occurs [2]. If the concrete's moisture level remains below a critical threshold, reinforcement corrosion proceeds at negligible rates even at conditions in carbonated concrete where the steel is depassivated [3]. As demonstrated in the Cemsuisse project 202004 [4], temporary wetting events – especially relevant for the exposure class XC4 – strongly influence moisture transport through the concrete cover and interact with electrochemical corrosion processes at the steel surface.

Based on these findings, we conclude that there are valuable opportunities to shift the focus away from carbonation resistance toward moisture and moisture transport control. We adopt the perspective that carbonation can be acceptable provided that the moisture state ensures sufficiently low corrosion rates. Thus, we consider moisture and corrosion rates as the more relevant parameters for durability design than the carbonation resistance.

2 Research objective

The aim of this project was to propose a new concept of ensuring the durability of reinforced concrete in XC exposure, capable of reflecting better the performance of reinforced concrete under service conditions than the current normative approach that is almost exclusively based on the carbonation resistance and thus tends to disadvantage cements with low GHG emissions. This new durability-design-concept shall shift the focus from understanding the concrete cover primarily as a barrier against carbonation (current approach) to understanding the concrete cover also as a barrier against moisture ingress during wetting (rain, splash water, etc.).

Thus, the objectives of this project were:

- Identify simple and suitable laboratory test methods to allow for characterizing and/or screening the barrier function of carbonated concrete against moisture penetration.
- Develop a conceptual procedure to analyze these test results towards ensuring that negligible corrosion damage occurs over the lifetime of a structure.
- Identify a combination of moisture transport characterization testing and model-based analysis, which could serve as a proposal for a future concept to be implemented in international standards.

3 Review of techniques to assess water permeability

In this project, we firstly reviewed different experimental techniques to determine moisture transport properties, moisture content and moisture state of concrete. The full literature review is included in appendix **Fehler! Verweisquelle konnte nicht gefunden werden.**, and the conclusions and recommendations are briefly provided here.

The mechanisms of moisture transport reviewed include permeation, diffusion, adsorption-desorption-condensation, and evaporation. The document examines various methods for measuring moisture transport properties in concrete, particularly those related to liquid transport coefficients such as sorptivity and permeability. Commonly used tests to assess water absorption and transport include the Initial Surface Absorption Test (ISAT), Figg and Covercrete absorption tests, and poroscope methods. While these tests are generally straightforward, their results can be affected by the initial moisture content and the challenge of ensuring unidirectional water ingress.

Additionally, the appendix reviews the approaches for determining moisture content in cementitious materials. Nuclear Magnetic Resonance (NMR) allows for depth-resolved water measurement by detecting hydrogen nuclei, while radiographic methods - utilizing X-rays, gamma rays, or neutrons - evaluate moisture distribution based on radiation attenuation. Electrical resistance measurements reflect moisture transport by monitoring changes in resistivity. Mathematical models simulate moisture movement using transport coefficients, and water vapor sorption isotherms estimate equilibrium moisture content based on relative humidity measurements. Each method presents unique advantages and limitations for assessing moisture in concrete and related materials.

The following criteria were initially defined to select the most feasible techniques:

1) the technique shall be capable of quantifying the liquid water at high RH or near-saturation conditions,
2) be applicable to bulk concrete (as opposed to cement paste or mortar),
3) be feasible for implementation (in terms of complexity, duration, equipment needed, and interpretation of results) in the laboratory of material testing institutes as routine tests,
4) provide data suitable for being extended to the long term and applied to different moisture conditions (e.g. by means of model-based approaches).

Based on the above criteria, the so-called “water absorption test” is selected to study liquid water transport in concrete. This is a widespread test method, also standardized in different countries. In Switzerland, the test is known as “Wasserleitfähigkeit” in standard SIA 206-1.

The appendix further shows that the so-called inverse analysis method can be used to indirectly determine the moisture transport coefficient (e.g., water permeability) based on the water absorption test. The relationship between external moisture condition (relative humidity) and internal moisture content can be quantified by measuring the water vapor sorption isotherms and the saturated salt solution method is suggested as it is more representative and feasible for lab tests than other methods.

4 Materials and methods

The experimental work of this project consists of repeating the experiments of Cemsuisse Projekt 202004 and new experiments of Cemsuisse Projekt 202204, which are described in this document.

4.1 Samples

The experimental plan includes the experiments and samples summarized in Figure 1:

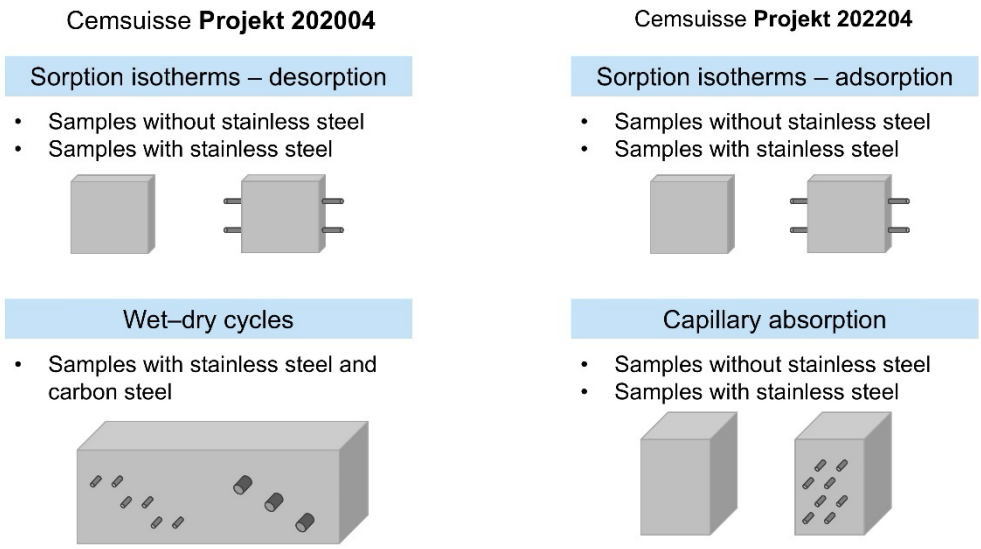

Figure 1 – Summary of experiments.

4.1.1 Mix design

The mortar samples were produced with the cement types and water/binder (w/b) ratios listed in Figure 2. A reduced experimental plan was chosen for Cemsuisse Projekt 202204, focusing on cement types more widely used (CEM II B-M (T-LL) is common only in Switzerland), and with lower w/b ratio 0.5, which is the upper limit defined in EN 206-1 for reinforced concrete structures under wet-dry cycles. The sand used had 4 mm maximal grain size, and sand-to-binder ratio 3:1 in all cases.

Figure 2 - Summary of mix design.

Each mix was prepared in batches of 5 kg (~ 2.3 litres) using a tabletop mixer according to the following protocol.

a) Prepare the moulds, clean the steel bars with ethanol and dry them. The moulds were 3D printed and no oil is used to avoid altering the surface.

b) Mix dry materials (sand and binder) for 1 minute at the low speed
c) Add water and mix for 2 minutes at low speed
d) Wait 2 minutes
e) Mix for 1 minute at the high speed
f) Fill moulds in layers
g) Vibrate on a vibration table until no more bubbles appear (ca. 20 seconds)

4.1.2 Curing

The samples were cured in a climate chamber at 95% RH. The curing duration depended on the binder, as shown in Table 1.

Table 1 – Curing durations for the four binder types.

CEM I	CEM II B-LL	CEM II B-M (T-LL)	CEM III B
28 days	56 days	56 days	91 days

4.1.3 Carbonation

All the specimens were carbonated prior to conducting the measurements. This was achieved in a carbonation chamber at 4% CO_2, 60% RH, and 20 °C. To probe the carbonation depth, additional reference prisms (4×4×16 cm^3) were produced from the same batches. These were periodically split (by means of a tensile test with 3 supports) and sprayed with the pH indicator phenolphthalein to assess the carbonation depth.

The approximate time to fully carbonate the reference prisms is shown in Table 2. Note that since for the slower carbonating samples, more time passed between the later carbonation checks, these values are an upper limit. Nevertheless, we can clearly observe that both higher w/b ratio and clinker replacement significantly increase the carbonation rate.

Table 2 - Approximate time (in days) passed to fully carbonate the prisms in the carbonation chamber for the 8 mixes investigated.

CEM I 0.5	CEM I 0.6	CEM II B-LL 0.5	CEM II B-LL 0.6	CEM II B-M (T-LL) 0.5	CEM II B-M (T-LL) 0.6	CEM III B 0.5	CEM III B 0.6
667 d	124 d	199 d	68 d	405 d	109 d	412 d	116 d

For all mixes, increasing the w/b ratio from 0.5 to 0.6 decreased the time to carbonate by a factor between 2.9 and 5.4. The mix CEM I with a w/b ratio of 0.5 took the longest to carbonate with almost two years, and the mixes CEM II B-M (T-LL) and CEM III B mixes with a w/b ratio of 0.5 also carbonated rather slowly. Among the four binders used, CEM II B-LL carbonated the fastest.

4.2 Cemsuisse Projekt 202004 specimens

For each of the 8 mixes considered in Cemsuisse Projekt 202204, the following experiments were conducted.

4.2.1 Wet-dry cycles

The samples of type A were exposed to wet-dry cycles with the goal of monitoring the mortar resistivity determined by impedance measurements, and the corrosion potential and corrosion

rate of embedded carbon steel bars. The sides of the samples were coated with epoxy resin after carbonation and before the wet-dry cycles. A schematic drawing of specimen A is shown in Table 3.

Table 3 - Samples for wet-dry cycles

Specimen type	Exposure history	No. of samples
Type A 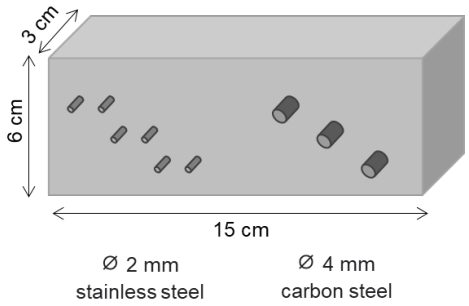	conditioned at 85% RH ↓ cyclic contact to water layer for capillary absorption	2 replicates per mix

Type A specimens had two types of steel bars embedded:

a) Three pairs (6 in total) of stainless-steel bars (⌀ 2 mm) at heights of 10, 20, and 30 mm from the bottom. Continuous measurement of the impedance between these pairs was performed to obtain the time evolution of the mortar resistivity at the three selected heights during the wetting and drying phases.

b) Three carbon steel bars (⌀ 4 mm), at the same heights – 10, 20, and 30 mm. They were used to monitor the corrosion potential during the dry/wet exposure. Additionally, their instantaneous corrosion rate was obtained via a linear polarization resistance (LPR) measurement at selected times during the experiment.

For each mix, two identical specimens were produced.

4.2.2 Sorption isotherms: desorption

For all eight mixes considered in Cemsuisse Projekt 202004, the sorption isotherms of the carbonated mortars were measured for the desorption path. To relate the sorption isotherms to impedance measurements, as well as studying a potential effect of the steel-concrete interface, specimens with and without embedded stainless steel bars were studied.

To facilitate casting and avoid the wall effect that could occur in thin samples, larger samples were produced using standard 4x4x16 cm molds (Type B, without steel bars) and 3D printed molds that accommodate the stainless steel (⌀ 2 mm) reinforcement (Type C). After carbonation, these samples were sliced using a wet cutting machine to produce Type B' and C' specimens, as presented in

Table 4. After cutting, the specimens were vacuum saturated with water and immersed overnight, then conditioned at different RHs, and finally dried in an oven at 65°C. The masses of these samples were monitored until equilibrium under each RH condition.

Table 4 – Samples for sorption isotherms – desorption.

Specimen type	Exposure history	No. of samples
Type B **Type B'** 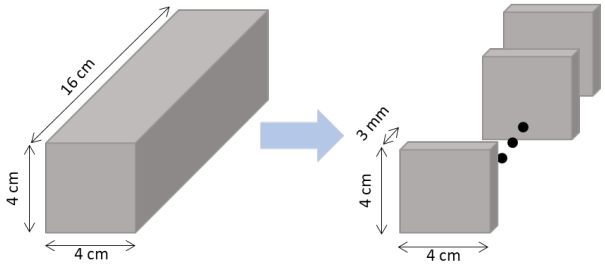	vacuum saturation ↓ 22%, 33%, 44%, 53%, 75%, 85%, 97% ↓ oven drying	3 replicates per RH 21 samples per mix
Type C **Type C'** 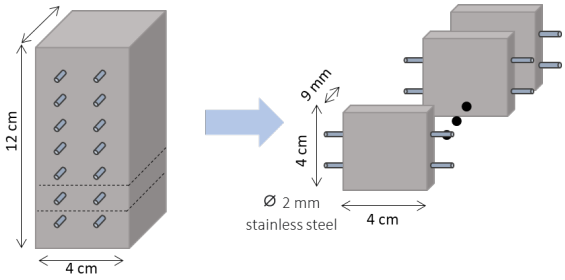	vacuum saturation ↓ 53%, 75%, 85%, 97% ↓ oven drying	3 replicates per RH 12 samples per mix

For the unreinforced samples, the RH conditions included a wider range (0%, 22%, 33%, 44%, 53%, 75%, 85%, 97%, 100% RH). However, the low conductivity at low saturation (associated with low RH) makes the impedance measurements unreliable. Thus, the type C' specimens were only measured for RH conditions higher than 53%.

By means of precise weight measurements, the water saturation (S) of the samples can be determined at the various levels of RH by comparing the weight with that in the saturated and dry state, as follows:

$$S = \frac{(\text{weight at RH}) - (\text{dry weight})}{(\text{saturated weight}) - (\text{dry weight})} \qquad \text{Equation 1}$$

This leads to S between 0 (dry) and 1 (saturated). The sorption isotherm is then generated by drawing the saturation values against the corresponding RH.

4.3 Cemsuisse Projekt 202204 specimens

4.3.1 Sorption isotherms: adsorption path

Sorption isotherms were also measured for Cemsuisse Projekt 202204, now considering the adsorption path, as well as the reduced group of mix designs. The production of the samples followed the same procedure described in section 4.2.2. The samples also included unreinforced (B') and reinforced (C') samples, as shown in Table 5.

To follow the adsorption path, the carbonated samples were first kept in an oven at 65°C until mass equilibrium and then stored at desiccators with varied RH and finally kept at vacuum

saturation at 100% RH. The masses of these samples were monitored until equilibrium in each RH condition, which can be later related to the degree of saturation of the samples.

Table 5 – Samples for sorption isotherms – adsorption.

Specimen type		Exposure history	No. of samples
Type B	**Type B'**	oven drying ↓ 22%, 33%, 44%, 53%, 75%, 85%, 97% ↓ vacuum saturation	3 replicates per RH 21 samples per mix
Type C	**Type C'**	oven drying ↓ 53%, 75%, 85%, 97% ↓ vacuum saturation	3 replicates per RH 12 samples per mix

4.3.2 Capillary absorption

The capillary absorption experiment consisted of exposing the samples to liquid water, subjecting them to water ingress by capillarity. Two types of samples, namely, unreinforced (Type D) and reinforced (Type E), were considered, as shown in Table 6. The samples consisted of rectangular prisms of 40 × 30 × 55 mm^3. For both Type D and Type E samples, the sides were coated with epoxy resin after carbonation, before the capillary absorption tests. The type D samples have four pairs of stainless steel rods (⌀ 2 mm) embedded at heights of 15, 25, 35, and 45 mm. Each pair was placed 12 mm apart center-to-center, such that the edge to edge distance was 10 mm. The pairs are positioned slightly offset to minimize the effect of lower stainless steel rods on the capillary transport of water.

Table 6 - Samples for capillary absorption

Specimen type	RH	No. of Samples
Type D 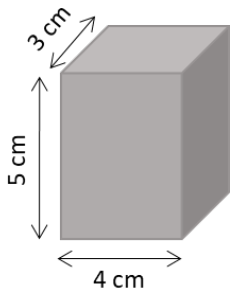	conditioned at 85% RH ↓ water layer for capillary absorption	3 replicates per mix
Type E 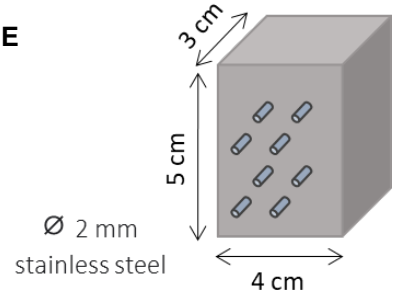	conditioned at 85% RH ↓ water layer for capillary absorption	3 replicates per mix

For the Type D samples, only the mass over time was recorded, whereas for the type E samples, both mass and impedance measurements on four channels were conducted. Measuring the weight of both samples aimed to show the effect of the steel and the SCI on the capillary absorption, as well as create a relationship between the mass gain and the water penetration depth that can be inferred from a drop in the impedance.

4.4 Summary of samples

The summary of all samples produced for each mix design is presented in Table 7.

Table 7 – Summary of characteristics of samples

Sample	Size (mm3)	Metals	Replicates/mix/phase	No. samples
A	150x60x30	6 ⌀ 2 mm stainless steel ⌀ 4 mm carbon steel	2	16
B	40x40x160	-	1 (+1 to check carb depth)	
B'	40x40x3	-	21	252
C	40x30x120	14 ⌀ 2 mm stainless steel	2	
C'	40x30x9	2 ⌀ 2 mm stainless steel	12	144
D	40x50x30	-	3	12
E	40x50x30	8 ⌀ 2 mm stainless steel	3	12

4.5 Corrosion measurements

The Type A specimens were used to monitor the corrosion potential and the resistivity of the mortar when exposed to cyclic wetting and drying. In addition, Linear Polarization Resistance

measurements (LPR) were performed to determine the evolution of the instantaneous corrosion rate.

The wetting phases and the dry periods in between are shown in Figure 3. The choice of cycle durations was motivated by meteorological data, which showed that most rain events last shorter than 3 hours. The additional 8-hour wetting cycle can be regarded as a rare longer rain period that leads to unusually high moisture levels.

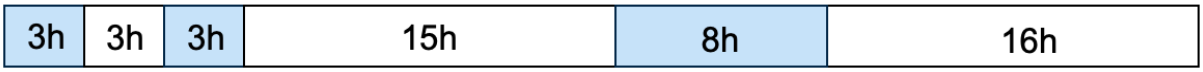

Figure 3 – Wet and dry cycle durations.

Before the experiment, the specimens were stored at 85% RH in a desiccator until constant mass. After a first measurement cycle under the initial conditions, the first wetting phase began. During the wet periods, the bottom of the mortar specimen was in contact with water, causing water ingress through capillary absorption. To consider varied reinforcement cover depths, the corrosion potential and corrosion rate of carbon steel rebars placed at three cover depths (10, 20, 30 mm) were monitored, alongside mortar resistivity measurements at these heights.

During these experiments, the corrosion potential (open circuit potential, OCP) of the carbon steels at different heights was monitored in relation to an external reference electrode (Ag/AgCl sat. KCl). To determine the corrosion rates, the carbon steel was polarized up to ±15 mV vs. OCP (LPR measurement). Electrochemical impedance spectroscopy (EIS) measurements at high frequencies were performed to determine the mortar resistance between the reference electrode and the working electrode, necessary to correct the resistance values obtained from the LPR measurement. The counter electrode was one of the stainless-steel bars embedded in the mortar.

The remaining stainless-steel bars were used for impedance measurements at 1 kHz, where the impedance was measured between each pair of stainless steel bars at the same height. From the impedance, the mortar resistivity can be estimated by accounting for the geometry factor, which can be obtained via numerical simulation. This was done using the finite element software COMSOL Multiphysics (see the details in Section 6.4).

The detailed measurement protocol is shown in Table 8. It was designed to obtain one corrosion rate measurement per hour for each of the three carbon steel bars, while the OPC is determined in between measurements.

Table 8 – Measurement protocol during the cyclic wet/dry exposure of the type A specimens.

	Channel	Measurement	Parameters	time	Cumulative time
7 cycles	1	OCP		1 min	1 min
	1	EIS	5 kHz -> 1 Hz, 15 mV, 7 points per decade	1 min	2 min
	1	LPR	±15 mV, scan rate 0.1667 mV/s	4 min	6 min
	1	Quick OCP		40s	
	2	Quick OCP		40s	
	3	Quick OCP		40s	20 min
	2	OCP		1 min	21 min
	2	EIS	5 kHz -> 1 Hz, 15 mV, 7 points per decade	1 min	22 min

7 cycles	2	LPR	±15 mV, scan rate 0.1667 mV/s	4 min	26 min
	1	Quick OCP		40s	
	2	Quick OCP		40s	
	3	Quick OCP		40s	40 min
	3	OCP		1 min	41 min
	3	EIS	5 kHz -> 1 Hz, 15 mV, 7 points per decade	1 min	42 min
	3	LPR	±15 mV, scan rate 0.1667 mV/s	4 min	46 min
7 cycles	1	Quick OCP		40s	
	2	Quick OCP		40s	
	3	Quick OCP		40s	60 min

5 Moisture transport modeling

For simulating moisture transport in cementitious materials, the multi-phase models are suggested as they can capture the interaction between different phases, while for simplification, the two-phase model, including liquid water and water vapor, was found to be enough to the mass changes during moisture transport [5–8]. Therefore, a two-phase continuum moisture transport model was employed in this project, which uses the established approach of homogenized simulations for mass transport in porous media [9]. The moisture transport is formulated by the Richards' equation, written as [5]

$$\frac{\partial S_l}{\partial t} = \nabla[D_a(S_l)\nabla S_l] \qquad \text{Equation 2}$$

with

$$D_a(S_l) = D_l(S_l) + D_v(S_l) \qquad \text{Equation 3}$$

where

$$D_l(S_l) = -k_{rl}\frac{K_l}{\phi\eta_l}\frac{\mathrm{d}P_c}{\mathrm{d}S_l} \qquad \text{Equation 4}$$

$$D_v(S_l) = -\left(\frac{M_v}{\rho_l RT}\right)^2 D_{v0}\phi^{x_D}(1-S_l)^{x_D+2}\frac{P_{vs}\mathrm{RH}}{\phi}\frac{\mathrm{d}P_c}{\mathrm{d}S_l} \qquad \text{Equation 5}$$

where $D_l(S_l)$ and $D_l(S_v)$ represent the diffusivity of liquid and vapor phases, S_l is the degree of liquid water saturation, k_{rl} is relative permeability, K_l is the intrinsic permeability, and x_D is a resistant parameter to consider the microstructural effect on vapor diffusion.

$D_a(S_l) = D_l(S_l) + D_v(S_l)$ The equilibrium between liquid water and water vapor is assumed because of the extreme slow moisture transport in a low permeable porous material [10]. The equilibrium between S_l and RH in the environment is represented by sorption isotherms, which are derived from the Kelvin equation and the van Genuchten equation [11],

$$S_l = \left[\left(\frac{P_c}{\alpha}\right)^{\frac{1}{1-m}} + 1\right]^{-m} \qquad \text{Equation 6}$$

where α and m are two material related parameters, determined by fitting the measured water vapor sorption isotherms, which were described in the previous sections (

Materials and methods).

The van Genuchten - Mualem model was used to calculate the relative permeability k_{rl} [11,12].

$$k_{rl} = S_l^{0.5}\left[1-\left(1-S_l^{\frac{1}{m}}\right)^{m}\right]^2 \qquad \text{Equation 7}$$

where m is taken from van Genuchten equation (see Equation 6).

The intrinsic water permeability, K_l is inversely determined by fitting the measured data to the simulated results. In this project, both the measured mass change curve and measured water distribution were used [13].

6 Results

6.1 Wet-dry cycles

The evolution of the steel potential during the wet-dry cycles, in terms of the variation of potential with respect to its initial values, is shown in Figure 4, calculated from the absolute values of corrosion potential, presented in Appendix A.1. Similarly, Figure 5 summarizes the evolution of the corrosion rate of steel during the wet-dry cycles. The mortar electrical impedance is plotted as absolute values in Figure 6, while Figure 7 shows normalized impedance values with respect to the ones at the start of the experiment. Notice that despite the noise in individual cases of the electrical resistivity data, a clear trend can still be observed.

The progressive effect of water ingress in the mortars is observed from the lower to the higher cover depths (10 mm < 20 mm < 30 mm). The data shows a cover depth dependent cascade of a decrease in the corrosion potential (Figure 4), an increase in the corrosion rates of steel (Figure 5), and a decrease in the mortar resistivity over time (Figure 6, Figure 7). Note that a shift of steel potential indicates a change in corrosion state of the metal. A pronounced negative shift of the potential usually indicates the transition from limited corrosion activity to increased corrosion activity. The electrical impedance is proportional to electrical mortar resistivity, a parameter that depends on multiple material properties, including porosity, pore structure, moisture state, and chemical composition of the liquid in the pores. Here, as we focus on the evolution over time, the primary influencing factor is the moisture state. The observed decreases of the impedance are thus suggestive of the arrival of moisture at the depth of the sensors (see below for a detailed discussion on these aspects).

Regarding the corrosion behavior of the different mixes, cements rank in increasing order of corrosion rates as CEM I, CEM II BM-TLL, CEM III, and CEM II B-LL, with increasing water-to-binder (w/b) ratio also leading to higher corrosion rates. This ranking is consistent with less pronounced drops in corrosion potential, higher initial mortar resistivity, as well as a less pronounced variation in resistivity over time.

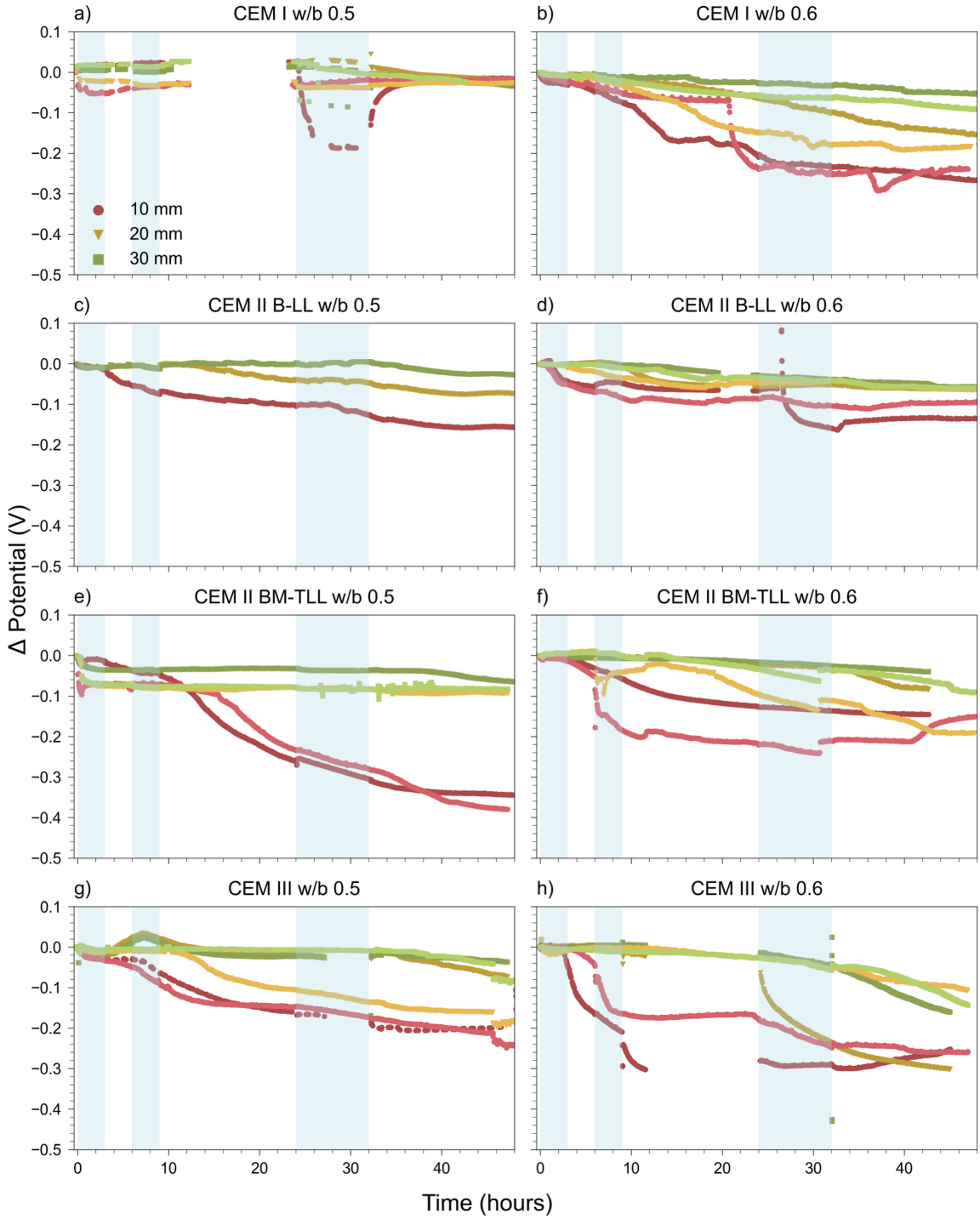

Figure 4 – Potential evolution during the wet-dry cycles. The blue shades indicate the wet periods (sample surface in contact with liquid water); the white parts correspond to the dry periods (sample surface exposed to indoor air).

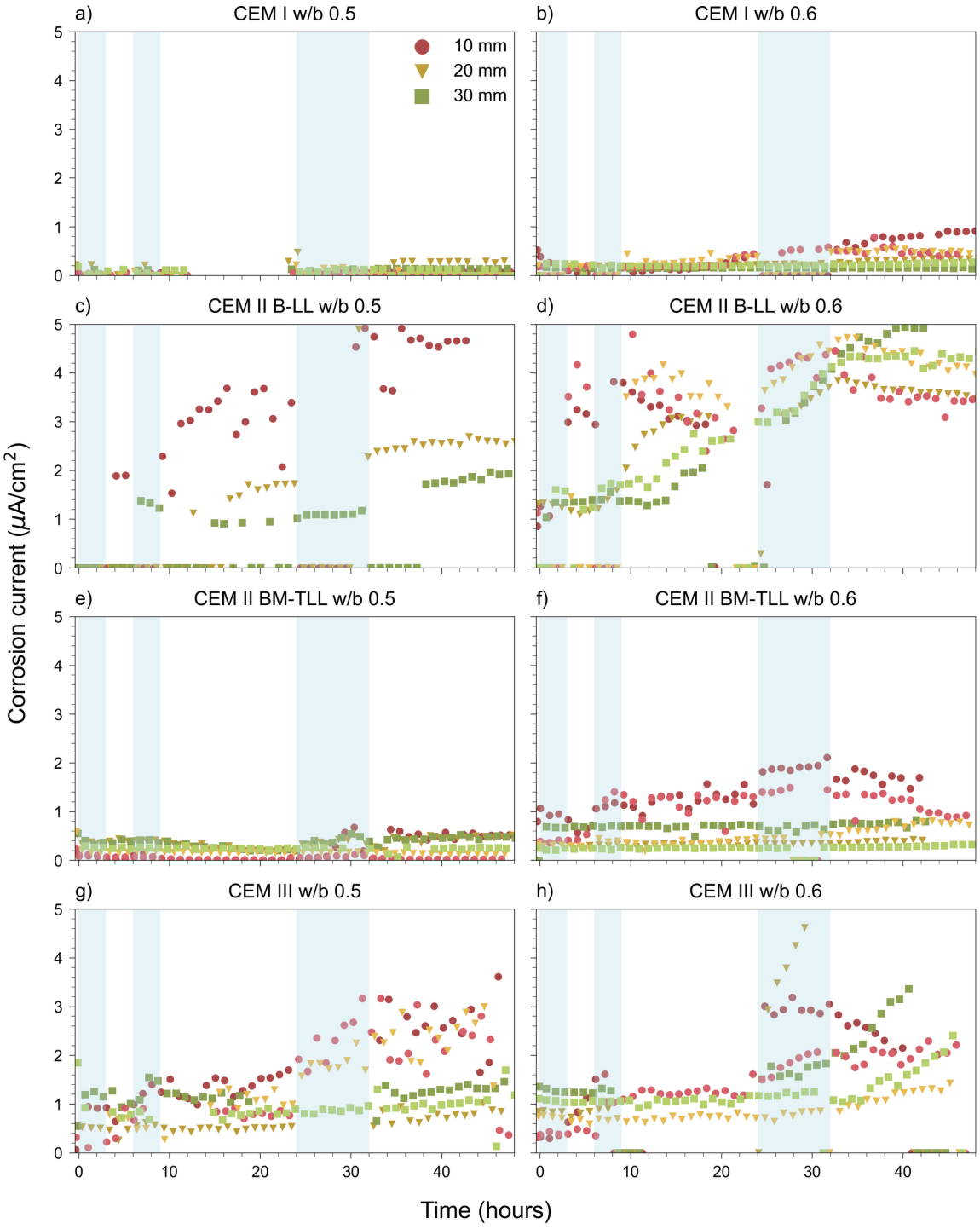

Figure 5 – Corrosion rate increases during the wet-dry cycles. The blue shades indicate the wet periods (sample surface in contact with liquid water); the white parts correspond to the dry periods (sample surface exposed to indoor air).

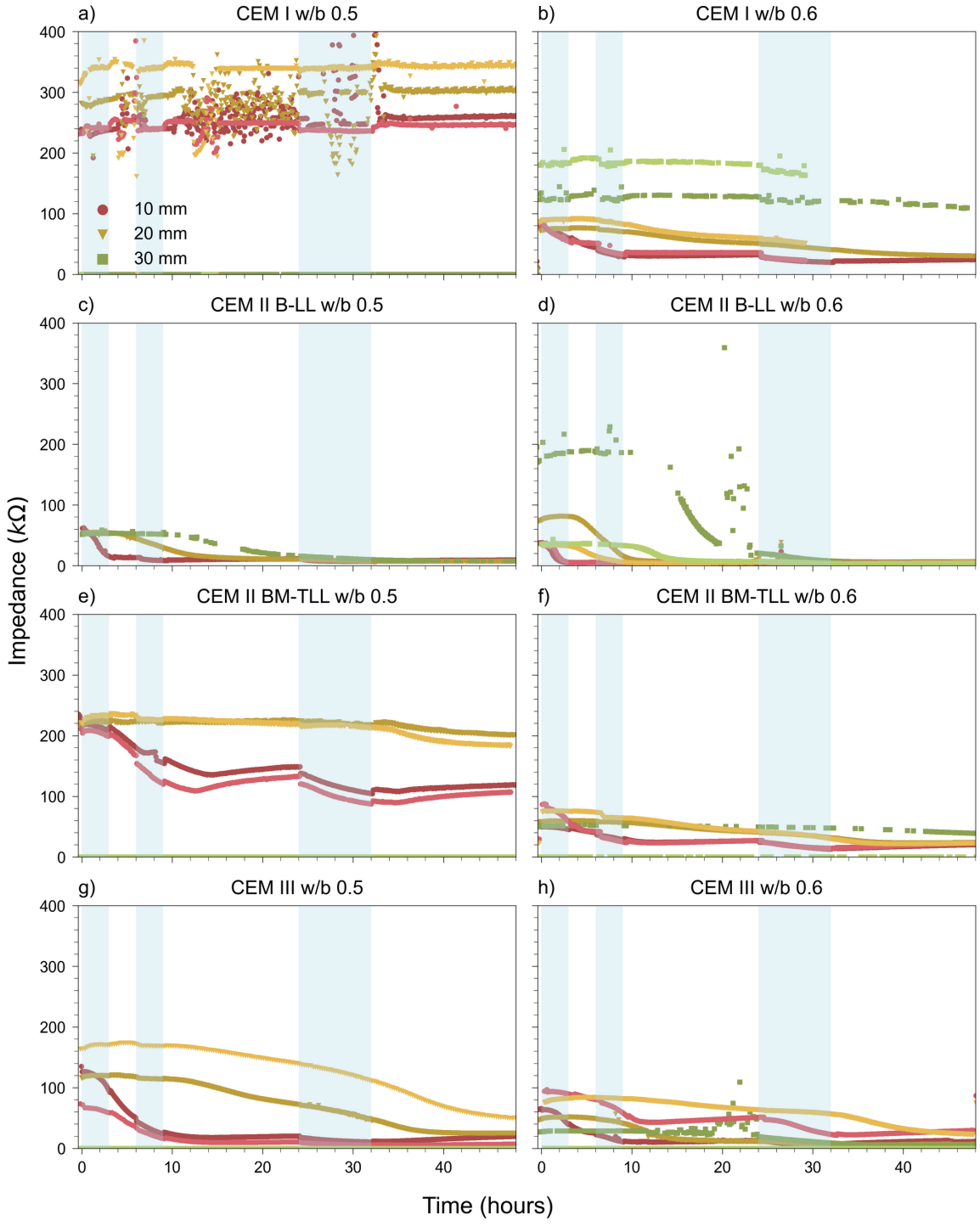

Figure 6 – Impedance evolution during the wet-dry cycles. The blue shades indicate the wet periods (sample surface in contact with liquid water); the white parts correspond to the dry periods (sample surface exposed to indoor air).

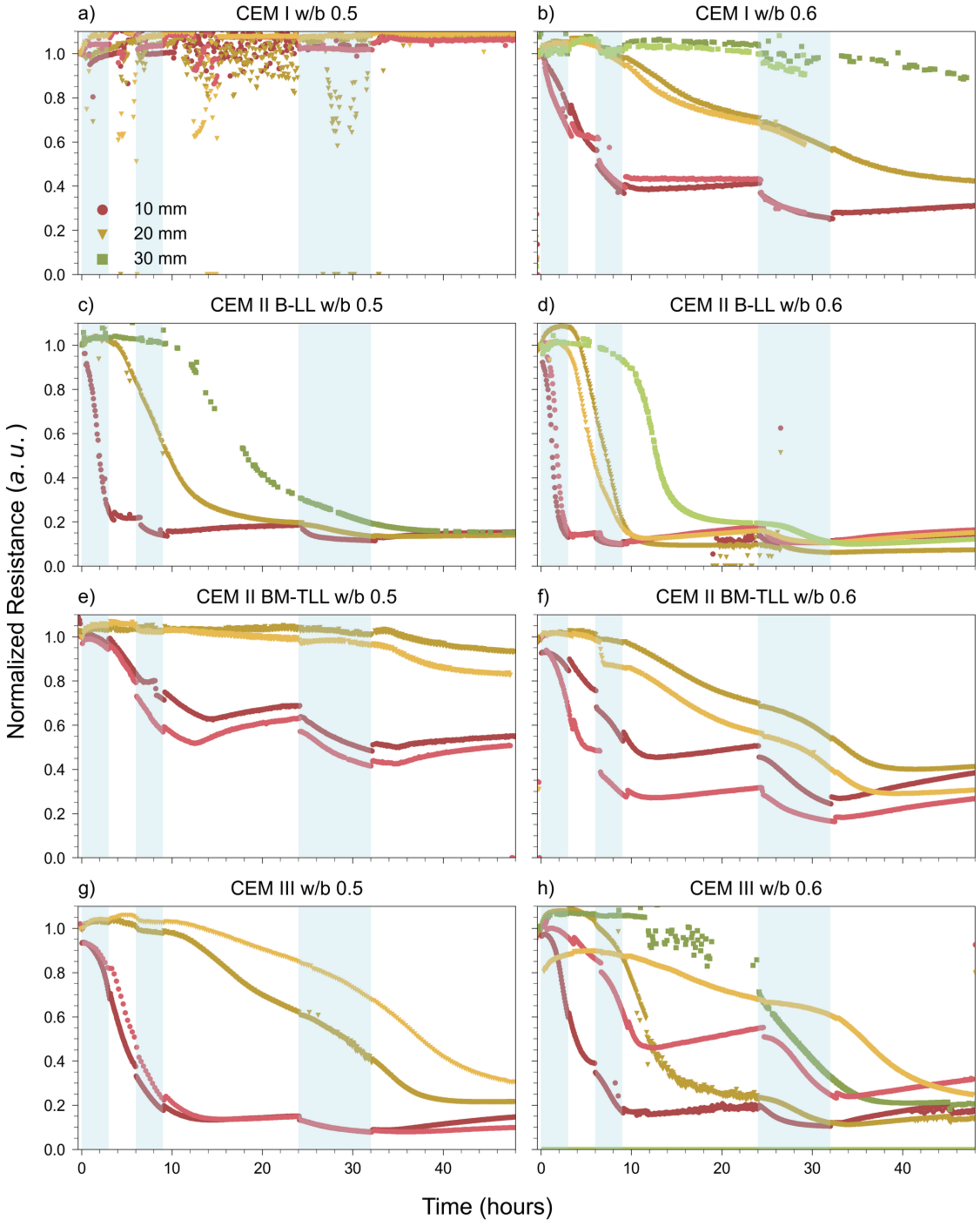

Figure 7 – Normalized resistance evolution during the wet-dry cycles. The blue shades indicate the wet periods (sample surface in contact with liquid water); the white parts correspond to the dry periods (sample surface exposed to indoor air).

6.2 Estimation of waterfront level

In the wet-dry cycle experiments, the mortar resistivity started to decrease before changes observed in the corrosion potential and corrosion rates of steel, even though both measurements are conducted with electrodes embedded at the same height. This indicates that the resistivity sensors appear to be able to capture the waterfront ingress earlier than the other types of measurements, and thus are sensitive to changes at depths shallower than the depth of the resistivity sensors. This is also reasonable since resistivity is measured between two electrodes embedded at the same depth by means of an imposed voltage signal. As a result, the measured resistivity can be expected to start decreasing when water reaches the lower part of this sensing area and equilibrates when the water overcomes its upper part. Such an intermediate point in the resistivity drop curve is thus interpreted to correspond to the water reaching the depth of the sensors. The time associated with this intermediate point of the resistivity drop correlates well with the time for the steel corrosion response, as shown in Figure 8.

In contrast to the resistivity measurements, the corrosion potential and corrosion rate would only change due to the presence of moisture directly at the SCI, acting as a more reliable metric to indicate the position of the moisture front.

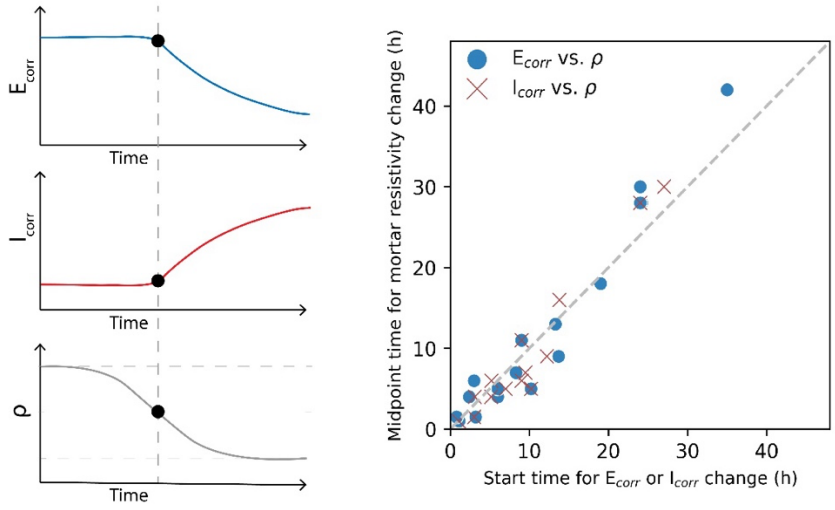

Figure 8 – An intermediate point of the resistivity drop curve correlates with the time for the start of the corrosion response of steel (corrosion potential decrease and corrosion rate increase), according to wet-dry cycles experiments.

Besides the experimental validation, a finite element simulation of the water ingress along a porous material with two embedded rebars confirms this hypothesis, as indicated in Figure 9. It shows that long before the more conductive domain reaches the steel bars, the impedance drops significantly.

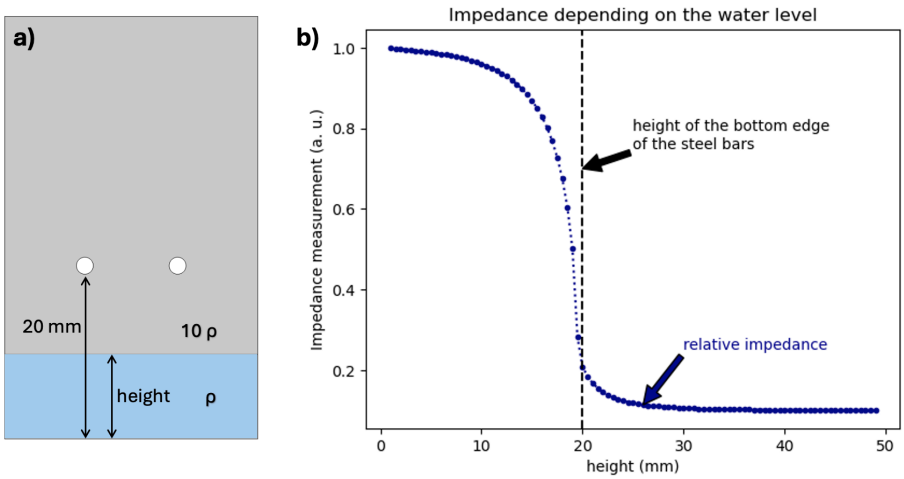

Figure 9 – Finite element simulation of electrical impedance evolution as water ingresses from the bottom of a porous material between two embedded sensors. a) Model setup: two separate mediums are considered, meant to represent dry and moist concrete. The lower one (moist) is assumed with a ten times lower resistivity than the upper (dry) one. The steel bars are at a height of 20 mm. b) Modeled impedance measurements for various heights of the lower medium.

6.3 Sorption isotherms

The sorption isotherms usually exhibit hysteresis, where for a given relative humidity, the desorption path leads to higher saturation values than the adsorption path. For the four mixes of Cemsuisse Projekt 202204, both adsorption and desorption paths were recorded and the results are provided in Figure 10, which shows that for CEM I 0.5, there is small hysteresis, while for the low-clinker mixes it is even smaller. This agrees with previous studies that have shown that carbonated concrete and mortar exhibit less hysteresis compared to uncarbonated ones due to changes in the porous microstructure that occur during carbonation [14,15].

While the adsorption path was only considered for the Cemsuisse Projekt 202204 mixes, the desorption path sorption isotherms were obtained for all eight mixes, as shown in Figure 11. It also shows the measurements recorded for the specimens containing a steel bar. These results show little difference between the values measured for the samples with steel and those without.

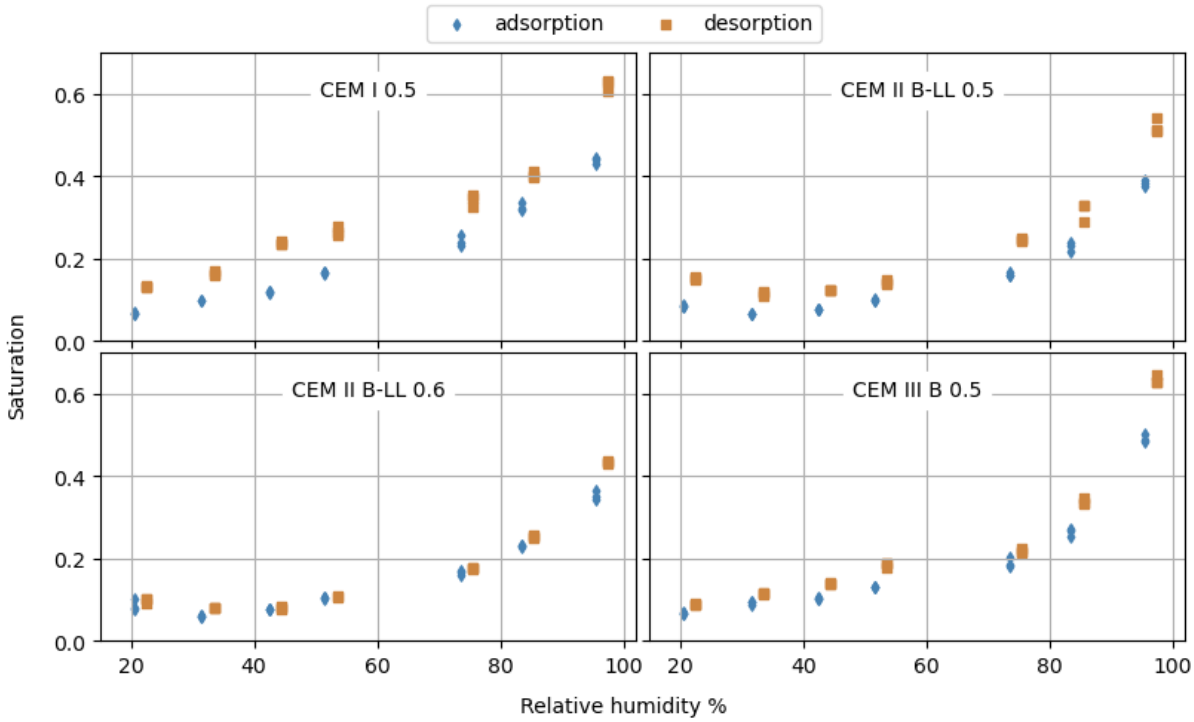

Figure 10 – Full sorption isotherms for the four mixes of Cemsuisse Projekt 202204.

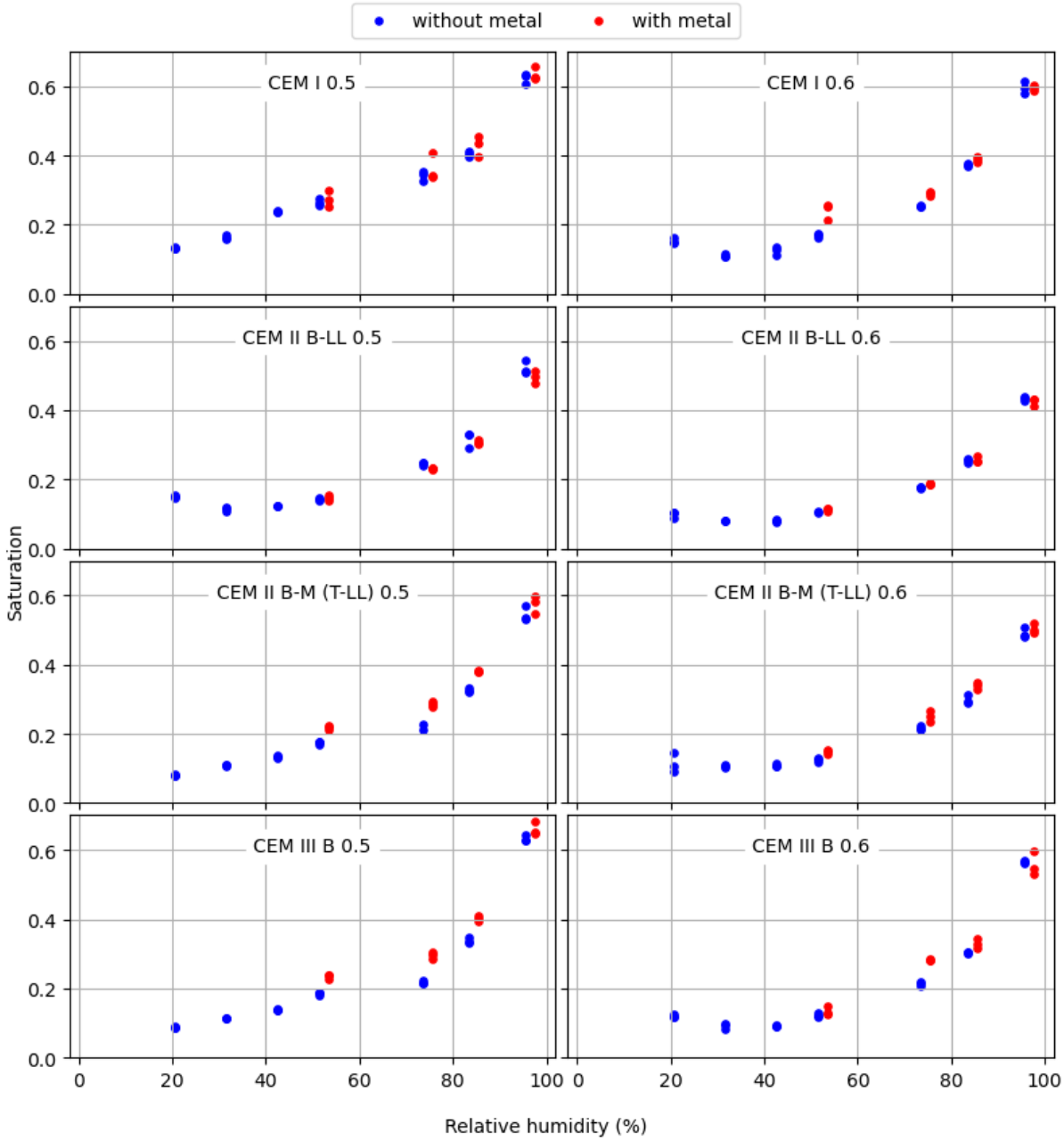

Figure 11 – Sorption isotherms for the desorption path showing the results for specimens with (Type C') and without (Type B') embedded stainless steel bars.

6.4 Mortar resistivity

The impedance measurements are dependent on the geometry, in particular the distance between the two electrodes, and their surface area. However, it can be used to compute the mortar/concrete resistivity, which is a material property. The conversion factor is sometimes referred to as cell constant, or geometry factor. By setting up a simple numerical model that

computes the current flow in a conductive media, this geometry factor can be obtained. In this case, with these specimens, the conversion from impedance Z to resistivity ρ is:

$$\rho = {}^{Z}/_{93.6\ \mathrm{m}^{-1}} \qquad \text{Equation 8}$$

Thus, for these specimens, a measured impedance of 100 kΩ translates to a resistivity of around 1 kΩm. This conversion factor was used to present the resistivity at saturated conditions in Figure 12.

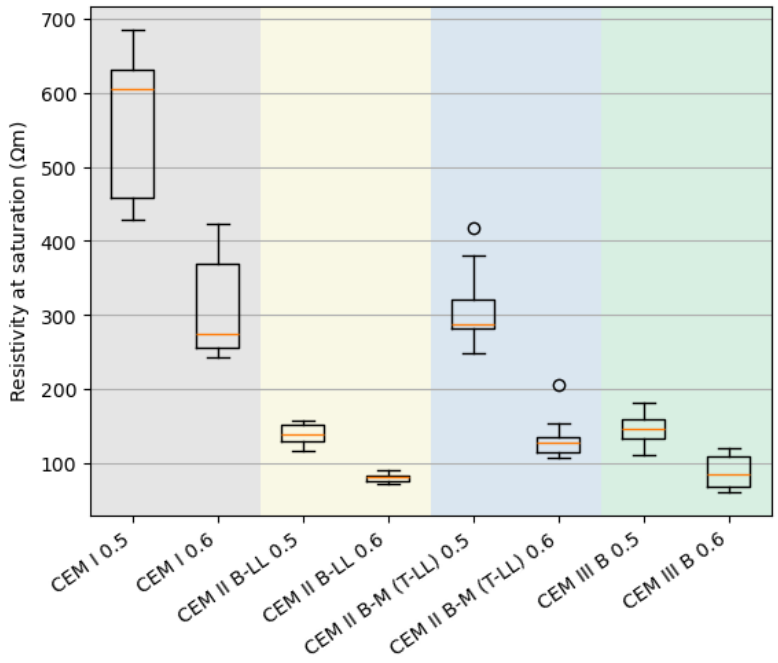

Figure 12 – Resistivity after vacuum saturation for the eight mixes considered (in carbonated state).

For the desorption path, the impedance values are shown in Figure 13. The values at saturation are drawn in the same figure, although it does not correspond to a certain relative humidity directly.

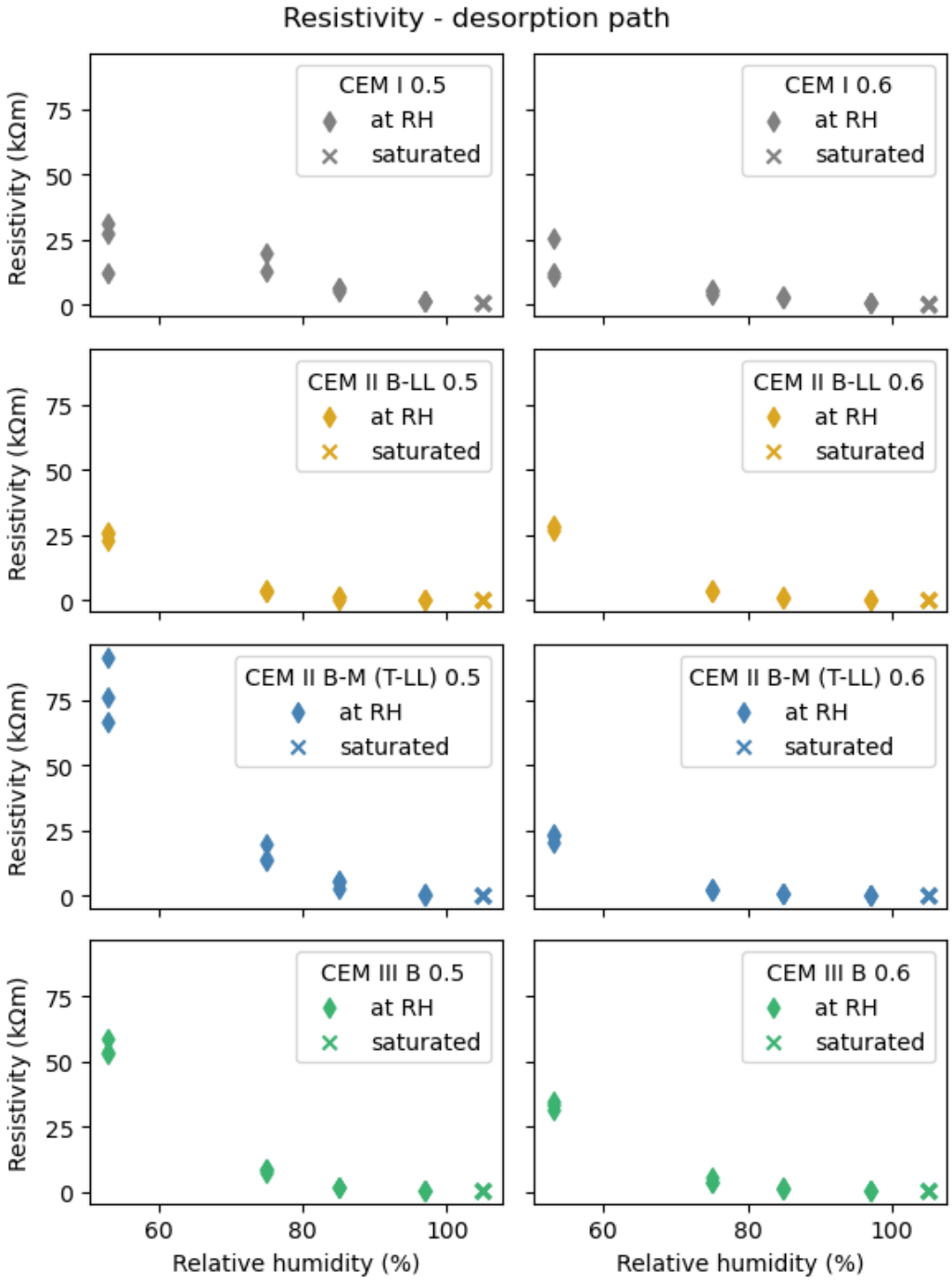

Figure 13 – Resistivity measured using the Type C' samples after conditioning them at certain relative humidity (in carbonated state).

For the adsorption path, the data is shown together with that of the desorption path for the four mixes of Cemsuisse Projekt 202204. For all mixes except for CEM I 0.5, the data overlap in many cases.

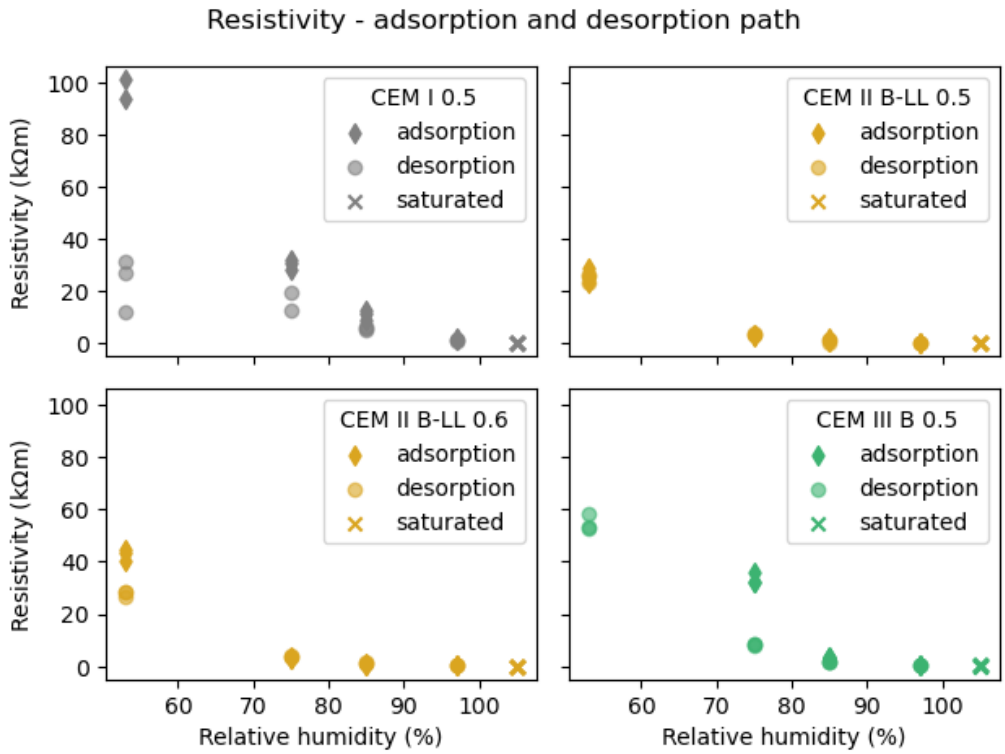

Figure 14 – Resistivity data obtained using the Type C' samples for both adsorption and desorption path (in carbonated state).

6.5 Capillary absorption

Selected samples were exposed to capillary water ingress experiments, monitoring the water gain in mass over time, as shown in Figure 15. The slope of this curve provides the mortar sorptivity, plotted in Figure 16. The mixes rank in order of increasing sorptivity as CEM I w/b 0.5, CEM III w/b 0.5, CEM II B-LL w/b 0.5, and CEM II B-LL w/b 0.6, corresponding to their increasing porosity due to the cement type and w/b ratio. The results also suggest a similar sorptivity for mixes that are unreinforced or reinforced. For CEM III and CEM II B-LL, the presence of a metal led to slightly higher total water absorption and sorptivity, whereas CEM I showed the opposite trend.

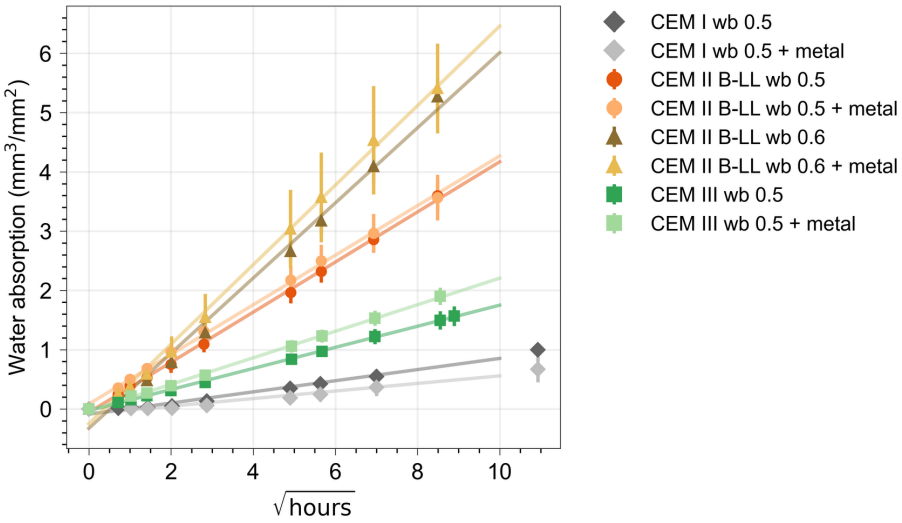

Figure 15 – Water absorption by capillary ingress over time for the different mixes in their carbonated state.

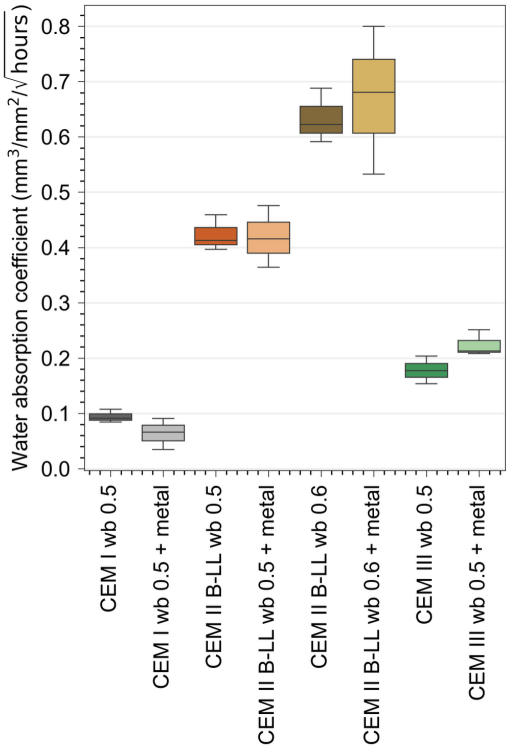

Figure 16 – Mortar sorptivity, calculated from the slope of the water absorption by capillary ingress over time, for mixes in their carbonated state.

The ingress of water was also monitored through impedance measurements (Figure 17), which showed a progressive decrease in resistivity from shallow to deeper cover depths as water reached the respective heights. Among the four mixes of Cemsuisse Projekt 202204, the CEM I w/b 0.5 showed the highest impedance, and it was the slowest to react to the water exposure. For 35 mm, there was no apparent impedance drop after 60 hours of water contact. The two

CEM II B-LL mixes with w/b of 0.5 and 0.6 already started at quite low impedance values in the initial condition (equilibrated at 85% RH), a factor between 5 and 10 times lower than the CEM I. From the impedance curves, one can clearly observe the delayed reaction for the higher cover depths. However, at all cover depths, the impedance drops significantly compared to the initial values over the course of the experiment, indicating a low resistivity caused by a high degree of saturation. For the higher cover depths, there is a higher variation in the time it takes for the impedance to drop. This is likely due to heterogeneous mortar microstructures, which cause slight differences in water transport between the replicate samples. In general, the impedance measurements of the CEM III B w/b 0.5 samples lie somewhere in the middle between the CEM I and the CEM II B-LL samples. For this mix, the highest cover depth of 45 mm remained relatively constant, with no reaction to the water, with the other three cover depths reacting more slowly than the CEM II B-LL samples, but still showing a clear drop in impedance.

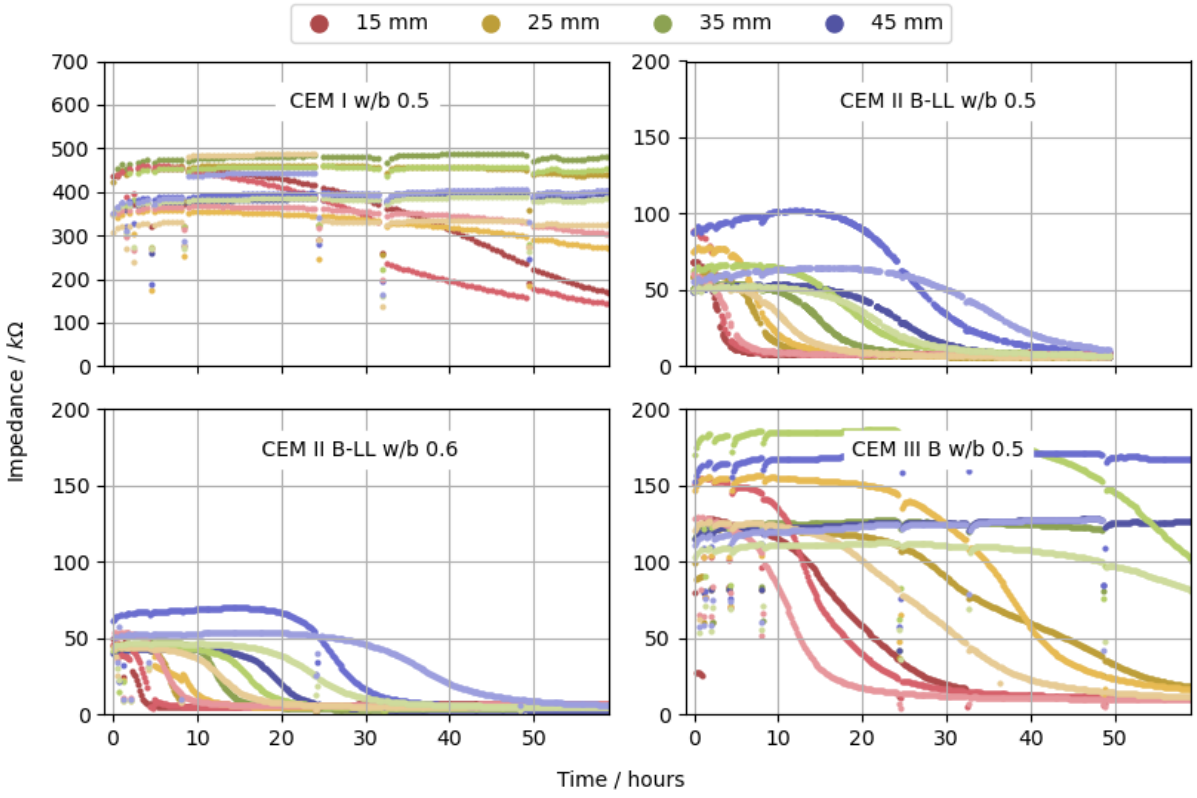

Figure 17 – Mortar impedance at different cover depths during water absorption by capillary ingress over time. Note the different scale of the y-axis for CEM I w/b 0.5 compared to that of the other three plots. The three replicate samples are shown in different brightness in no particular order.

6.6 Numerical analysis

6.6.1 Model calibration

The moisture transport model was calibrated by two different types of data, namely, measured mass change and measured impedance during water capillary absorption tests. If the measured impedance can well represent the process of water uptake, the calibrated results of the intrinsic permeability K_l with two types of data should be similar. Figure 18 shows the fitting results of simulated mass change to the measured mass increase during water capillary absorption for CEM B-LL w/b 0.5 and 0.6. For both materials, the simulated curves can well capture the measured mass increase curves, indicating the applicability of the moisture transport for the studied cementitious materials.

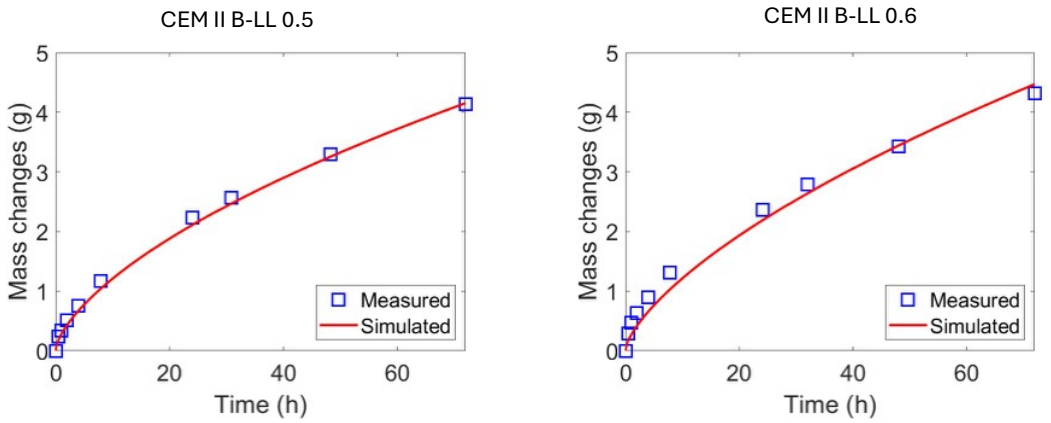

Figure 18 - Model calibration by fitting simulated mass change to the measured mass increase during water capillary absorption.

As discussed above (see Figure 8), the intermediate point of a measured impedance curve has a good correlation with the time when the measured steel potential and corrosion rate values suggest arrival of the moisture front. Therefore, we took the time at the intermediate point of the measured impedance curve and adjusted K_l to let water arrival time at the steel depths fit the intermediate point time. The simulated saturation profiles are shown in Figure 19, which should be compared with the impedance curves in Figure 17. As the results from three samples have a large scatter, the average of three samples was considered.

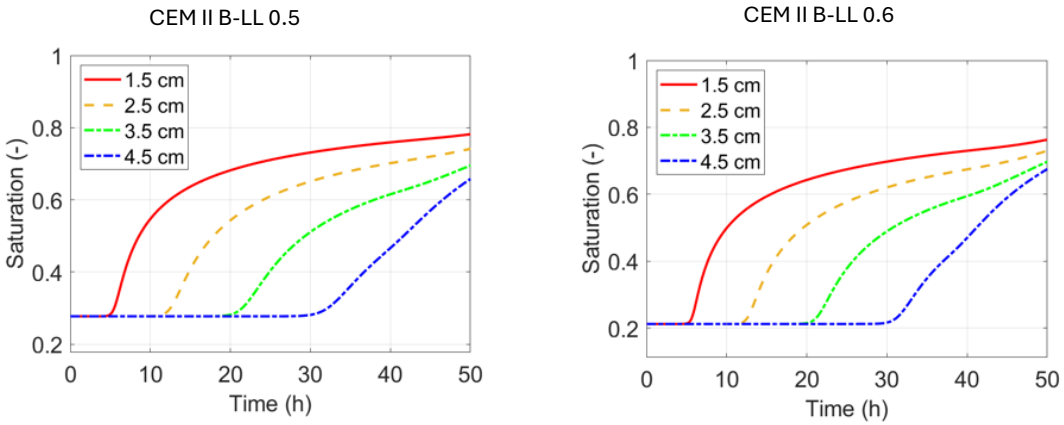

Figure 19 - The simulated saturation profiles based on the calibrated K_l based on the measured impedance during water capillary absorption.

The determined K_l are provided in Table 9, which K_l values calibrated by impedance are much higher (up to 10 times) than that by the mass increase curves. The discrepancy may be caused by the different types of samples (with and without steel bars, leading to specimens with somewhat different microstructure), although we do not consider it very likely that the presence of steel bars accelerates moisture transport as implied by the measured impedance. The most likely reason is that the impedance measurement is very sensitive to the moisture uptake, so that the impedance between two steel bars starts to decrease much earlier than the time of water arrival at the steel. This matter clearly needs more research, which, however, is beyond the scope of the current project.

Table 9 - The determined intrinsic permeability $K_l(m^2)$ by different types of data

Materials	Mass increase	Impedance
CEM II 0.5	8.95E-18	25 - 35E-18
CEM II 0.6	13.5E-18	50 - 140E-18

6.6.2 Simulation results of wet-dry cycles

After determining the values for K_l, the moisture transport simulations were run with the goal of replicating the wet-dry cycle measurements. Since the mass was not measured during the wet-dry cycles measurements, the simulated results can only be compared with the measured impedance curves, as shown in Figure 7. Therefore, the calibrated K_l with the impedance was used for the simulations and the simulated saturation profiles are shown in Figure 20. Comparing with curves in Figure 7, the saturation profiles in Figure 20 evolve very slowly. The measured impedance curves for steel bars at 2 cm and 3 cm sharply decrease at 10-20 hours and 20-30 hours, respectively, but there is no obvious decrease in the simulated saturation profiles. This further confirms our hypothesis that the measured impedance can detect water uptake much earlier than water reaches the steel bar.

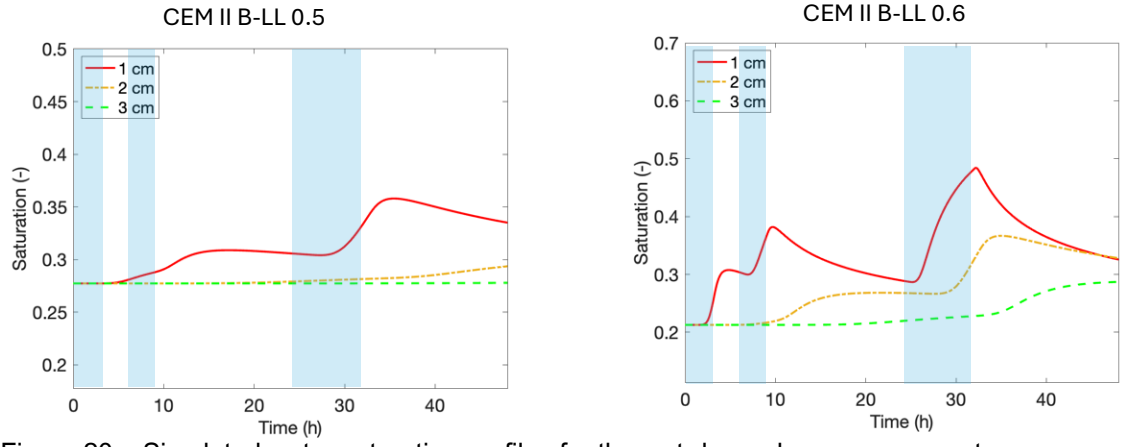

Figure 20 – Simulated water saturation profiles for the wet-dry cycles measurements.

7 Discussion

7.1 Wet-dry cycles

The aim of the wet-dry cycle experiments was to investigate the response time of the reinforcement to water exposure. The ingress of moisture was associated with a decrease of the mortar impedance, as well as a decrease in the corrosion potential and an increase in the corrosion rate of steel.

As expected, for all eight mixes, the cover depth was an important factor delaying the effects of the moisture ingress. Except for CEM I w/b 0.5, all the steels at 10 mm distance from the water showed a drop of the potential after the first two wetting phases. Likewise, the corrosion rate tended to rise most quickly for the lowest steel. By contrast, after two wetting phases, almost all the steels at 30 mm exhibited relatively stable potentials and corrosion rates for all binders and w/b ratios, with only the ones from the CEM II B-LL w/b 0.6 increasing significantly over the course of the experiment. This shows that for all four binders used in this experiment, adjusting the w/b ratio and the cover depth are possible strategies to limit the corrosion rate for realistic wetting scenarios.

Lower mortar impedances, more negative potentials and higher corrosion rates correlate qualitatively well, as exemplified in Figure 21. However, the correlation on the exact point in time when these properties start to change due to water ingress was less pronounced than expected. As discussed in Section 6.4, this is because the impedance measurement is affected not only by the moisture state at the level of the stainless steel bars themselves, but also the moisture state - which affects the conductivity and resistivity - in the surrounding material. Thus, the impedance reacted to moisture changes earlier than the potential and corrosion rate of steel, which are directly associated with the moisture state at the steel level.

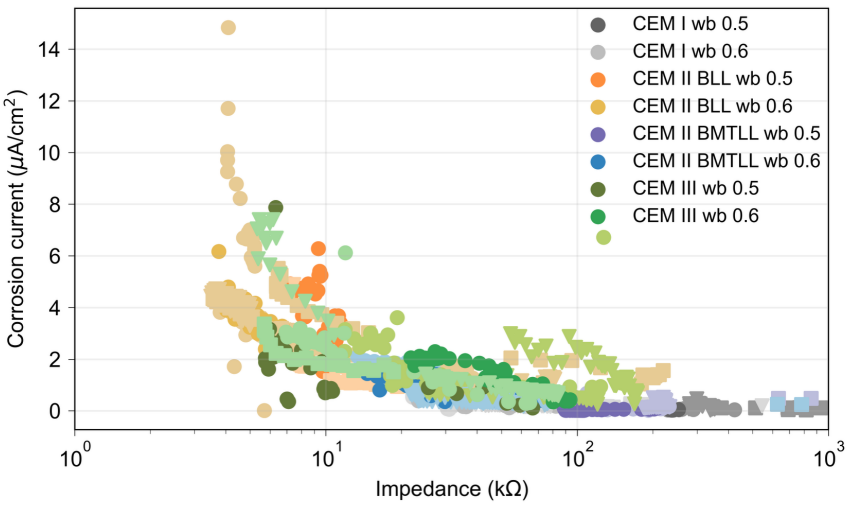

Figure 21 – Correlation between mortar impedance and corrosion current.

7.2 Sorption isotherms and resistivity measurements

The sorption isotherm experiments with the type C' specimens can be used to calibrate the measured impedance and moisture content. However, it is important to note that this relation is obtained at the moisture equilibrium state – since the specimen was at equilibrium after being

stored long enough in a desiccator – and not for dynamic situations such as in the wet-dry cycle experiment.

The resistivity and saturation relations are shown in Figure 22, which approximately follow this form:

$$S = a \cdot Z^b \qquad \text{Equation 9}$$

The fitting parameters are provided in Table 10. In all cases, the factor a is lower for the fit of the adsorption path data than that of the desorption path data. In Figure 22, this translates to a lower y-axis intercept, while the value of b represents the slope in the log-log plot. Thus, the desorption and adsorption paths lead to distinct relations.

Table 10 – Fitting parameters for the saturation–impedance relation.

Mix	**Path**	$\boldsymbol{a}$	$\boldsymbol{b}$
CEM I 0.5	desorption	2.55	-0.29
CEM I 0.5	adsorption	1.39	-0.23
CEM II B-LL 0.5	desorption	0.94	-0.24
CEM II B-LL 0.5	adsorption	0.76	-0.22
CEM II B-LL 0.6	desorption	1.02	-0.29
CEM II B-LL 0.6	adsorption	0.57	-0.19
CEM III B 0.5	desorption	1.05	-0.18
CEM III B 0.6	adsorption	0.90	-0.19

While the fitting works reasonably well in this situation, it is important to stress that this analysis is not directly applicable to other experiments performed in this project. Further information is required to treat dynamic situations with spatial and temporal variations in moisture content. Since the impedance is affected by the moisture distribution in a relatively large zone around the steel electrodes, as demonstrated in Figure 9, the distribution of water has to be estimated before the saturation can be determined.

Further investigations into the moisture transport are required to formulate an analogous relation to Equation 9 for dynamic situations. Previous studies have used neutron imaging to analyse the water ingress and the possible shapes of the waterfront [16]. Using such data, it might be possible to calibrate such a relation for capillary absorption scenarios. Nevertheless, it is possible to use Equation 9 as a first approximation.

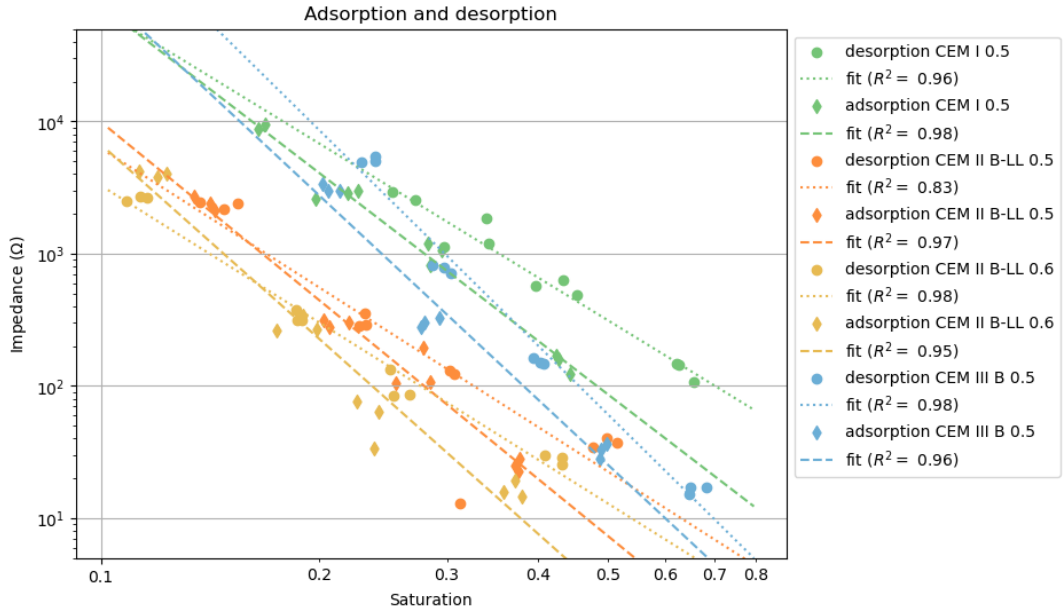

Figure 22 – Impedance and saturation for the Cemsuisse Projekt 202204 mixes showing the desorption and adsorption paths, and their linear fit.

7.3 Resistivity and clinker factor

The four binders used have different amounts of clinker replacement. Using approximate values for the clinker factor, Figure 23 shows that the resistivity increases with the amount of clinker used.

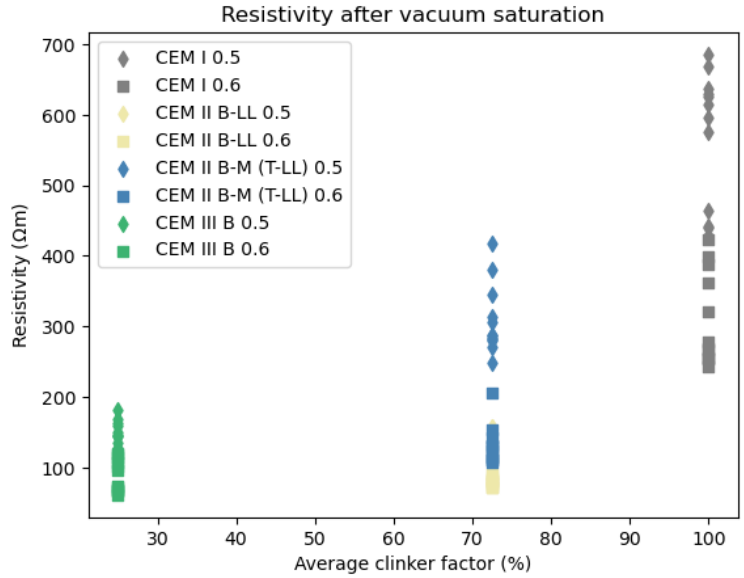

Figure 23 – Resistivity under saturated conditions and the approximate clinker factor of the mixes.

7.4 Experiments and test methods

The presented methods differ in complexity and application.

1) Impedance measurements are relatively simple, robust and fast, and thus already used on structures, for example, by means of embedded sensors or through non-destructive techniques (e.g. the Wenner probe). However, they generally serve as qualitative indicator, and, as explained in Section 0, it is complex to relate the moisture state at the steel - where it is most relevant - to the impedance measurement. Further experiments are required to link those two quantities.
2) Potential measurements are also straightforward and widely used in engineering practice, such as potential mapping. In the experiments of this project, the potential served as an indicator for the time when the moisture was reaching the steel. However, although some mixes had similar potential curves during the wet-dry cycle experiment, the corrosion rate behaved differently. Here too, more analysis is required for a comprehensive understanding.
3) LPR measurements are primarily used in a lab setting and require specialized equipment and a specimen equipped with appropriate electrodes. They can be used to determine the instantaneous corrosion rate and thus provide the reference to the other measured quantities. One possible goal would be to quantify parameter ranges for more easily measurable quantities that correspond to acceptable values of corrosion rate.
4) Capillary absorption tests are simple and already standardized. Thus, they would be a good candidate to explore a testing regime that quantifies corrosion risk based on the susceptibility to water ingress.
5) The use of numerical simulations is also a promising tool, especially if it can be calibrated using a series of standardized tests. As presented in Section 6.6.1, there are multiple calibration options and further finetuning is required. Here too, additional data would aid in validating the model.

Capillary absorption testing appears to be the most straightforward option for introducing an additional parameter. However, the current dataset is not comprehensive enough to establish definitive threshold values for classifying potential binders based on their corrosion risk due to moisture ingress. Nevertheless, the findings from this project generally reinforce the strategy of targeting moisture control to mitigate corrosion in reinforced concrete and provide a strong basis for future research in this area.

8 Conclusions

This project combined a number of experimental techniques, as well as numerical analysis, to investigate moisture transport and its effect on corrosion in carbonated mortars. Four binders with two water/binder ratios were studied. The results from this project show correlations between the measured quantities that substantiate the importance of moisture for corrosion of steel in carbonated concrete. The following major conclusions can be drawn:

1) The dynamic behavior upon wetting/drying exposure plays an important role in the durability of carbonated reinforced concrete. Upon wetting, moisture penetrates the concrete cover and once reaching the steel reinforcement – here assessed by electrical impedance measurements with embedded electrodes – significantly increases the corrosion rate of the steel.
2) If concrete remains dry at the steel cover depth, that is, if the moisture front does not reach the embedded steel upon a given wetting event, corrosion rates remain low for the studied mixes irrespective of cement type and w/b ratio.
3) Characterization of the water sorptivity of the different mortar mixes (after accelerated carbonation) supports the evaluation to what extent the material can delay water ingress and thus corrosion.
4) The mortar pore structure influences the corrosion rate after the moisture front reaches the steel (characterized by sorptivity): in high moisture conditions, corrosion rates are lower for less porous and less permeable mixes with CEM I and CEM II BM-TLL, and a lower w/b, compared to the more porous and permeable CEM III and CEM II B-LL mixes and at higher w/b. Among the here studied mixes, environmental conditions such as wetting with liquid water might become critical in terms of corrosion risk – leading to critical corrosion rates of the order of several tens of micrometers per year – for steel in carbonated concrete in CEM III and CEM II B-LL.
5) In addition to the ability of mortar resisting moisture ingress, additional material properties play a role. Certain materials, such as CEM III, might develop relevant corrosion rates of steel despite their low sorptivity. This could be due to additional factors, such as their pore solution composition, which were not explored further here.

Thus, **a new conceptual approach for laboratory testing** can be proposed. In the future, complementing pure carbonation resistance testing with testing for concrete sorptivity (in carbonated state) will allow to estimate the service life better. While carbonation testing assists in evaluating the corrosion initiation phase, sorptivity testing upon carbonation can assist in evaluating the corrosion propagation phase, namely to what extent exposure to wetting events (e.g. rain, splash water, etc.) will trigger corrosion of the steel embedded at a certain cover depth. To achieve this, capillary water sorption tests may be combined with moisture transport modeling, in order to simulate the ingress of water and forecast the degree of saturation at the steel depth as a function of relevant wet/dry scenarios.

However, further research is needed to develop and validate such an approach.

Note that the findings from this work are not necessarily applicable to other conditions, especially other binder types, mix proportions, carbonation conditions, and moisture exposure conditions.

9 Recommendations for further work

Water ingress monitored by electrical impedance measurements, as a robust and simple monitoring technique, provides an early indicator of corrosion risk but might overestimate the moisture state at SCI and the corrosion rate if not interpreted properly. In this regard, further research is needed to correlate moisture transport and concrete impedance monitoring.

Further research is also required to quantify steel corrosion rates as a function of degree of saturation (instead of exposure relative humidity). This requires complementary determination of corrosion rates (electrochemical measurements) and concrete-water interaction (e.g. sorption isotherms) on parallel specimens produced from the same mixes, upon carbonation. Such future research should also consider the dynamic behavior upon wetting and drying in addition to equilibrium states.

While the data presented here is encouraging with respect to a shift in future durability testing and standardization, the collected data is not sufficient to determine threshold values for engineering practice. In particular, as can be inferred from conclusion no. 5, “water saturation thresholds” at the steel to keep corrosion within acceptable boundaries would likely need to be stipulated based on the binder type. This will require extending the experiments over a wider range of binders and mix proportions.

10 References

[1] M. Schneider, The cement industry on the way to a low-carbon future, Cem Concr Res 124 (2019) 105792. https://doi.org/10.1016/J.CEMCONRES.2019.105792.

[2] C. Alonso, C. Andrade, J.A. González, Relation between resistivity and corrosion rate of reinforcements in carbonated mortar made with several cement types, Cem Concr Res 18 (1988) 687–698. https://doi.org/10.1016/0008-8846(88)90091-9.

[3] M. Stefanoni, U.M. Angst, B. Elsener, Electrochemistry and capillary condensation theory reveal the mechanism of corrosion in dense porous media, Sci Rep 8 (2018) 1–10. https://doi.org/10.1038/s41598-018-25794-x.

[4] T. Schmid, Z. Zhang, U. Angst, Ensuring the durability of reinforced concrete structures during carbonation and alternating wet/dry exposure, Zurich, 2023. https://www.cemsuisse.ch/app/uploads/2023/10/202004_Abschlussbericht-Stahlbetonbauten-bei-Karbonatisierung-Web.pdf (accessed November 26, 2025).

[5] Z. Zhang, M. Thiery, V. Baroghel-Bouny, Investigation of moisture transport properties of cementitious materials, Cem Concr Res 89 (2016) 257–268. https://doi.org/10.1016/j.cemconres.2016.08.013.

[6] J. Rymeš, I. Maruyama, A. Aili, Time-dependent water vapor desorption isotherm model of hardened cement paste, Cem Concr Res 150 (2021) 106612. https://doi.org/10.1016/J.CEMCONRES.2021.106612.

[7] J. Bao, R. Zheng, J. Wei, P. Zhang, S. Xue, Z. Liu, Numerical and experimental investigation of coupled capillary suction and chloride penetration in unsaturated concrete under cyclic drying-wetting condition, Journal of Building Engineering 51 (2022) 104273. https://doi.org/10.1016/J.JOBE.2022.104273.

[8] F. Ren, C. Zhou, L. Li, H. Cui, X. Chen, Modeling the dependence of capillary sorptivity on initial water content for cement-based materials in view of water sensitivity, Cem Concr Res 168 (2023) 107158. https://doi.org/10.1016/J.CEMCONRES.2023.107158.

[9] U. Hornung, Homogenization and Porous Media, Springer 6 (1997). https://doi.org/10.1007/978-1-4612-1920-0.

[10] M. Mainguy, O. Coussy, V. Baroghel-Bouny, Role of Air Pressure in Drying of Weakly Permeable Materials, J Eng Mech 127 (2001) 582–592. https://doi.org/10.1061/(ASCE)0733-9399(2001)127:6(582).

[11] M.Th. van Genuchten, A Closed-form Equation for Predicting the Hydraulic Conductivity of Unsaturated Soils1, Soil Science Society of America Journal 44 (1980) 892. https://doi.org/10.2136/sssaj1980.03615995004400050002x.

[12] Y. Mualem, A new model for predicting the hydraulic conductivity of unsaturated porous media, Water Resour Res 12 (1976) 513–522. https://doi.org/10.1029/WR012i003p00513.

[13] Z. Zhang, M. Thiery, V. Baroghel-Bouny, Numerical modelling of moisture transfers with hysteresis within cementitious materials: Verification and investigation of the effects of repeated wetting-drying boundary conditions, Cem Concr Res 68 (2015) 10–23. https://doi.org/10.1016/j.cemconres.2014.10.012.

[14] Z. Zhang, U. Angst, Microstructure and moisture transport in carbonated cement-based materials incorporating cellulose nanofibrils, Cem Concr Res 162 (2022) 106990. https://doi.org/10.1016/j.cemconres.2022.106990.

[15] M. Auroy, S. Poyet, P. Le Bescop, J.M. Torrenti, T. Charpentier, M. Moskura, X. Bourbon, Impact of carbonation on unsaturated water transport properties of cement-based materials, Cem Concr Res 74 (2015) 44–58. https://doi.org/10.1016/j.cemconres.2015.04.002.

[16] Z. Zhang, P. Trtik, F. Ren, T. Schmid, C.H. Dreimol, U. Angst, Dynamic effect of water penetration on steel corrosion in carbonated mortar: A neutron imaging, electrochemical, and modeling study, Cement 9 (2022) 100043. https://doi.org/10.1016/j.cement.2022.100043.

[17] M. Stefanoni, U. Angst, B. Elsener, Corrosion rate of carbon steel in carbonated concrete – A critical review, Cem Concr Res 103 (2018) 35–48. https://doi.org/10.1016/j.cemconres.2017.10.007.

A Appendix

A.1 Corrosion potential

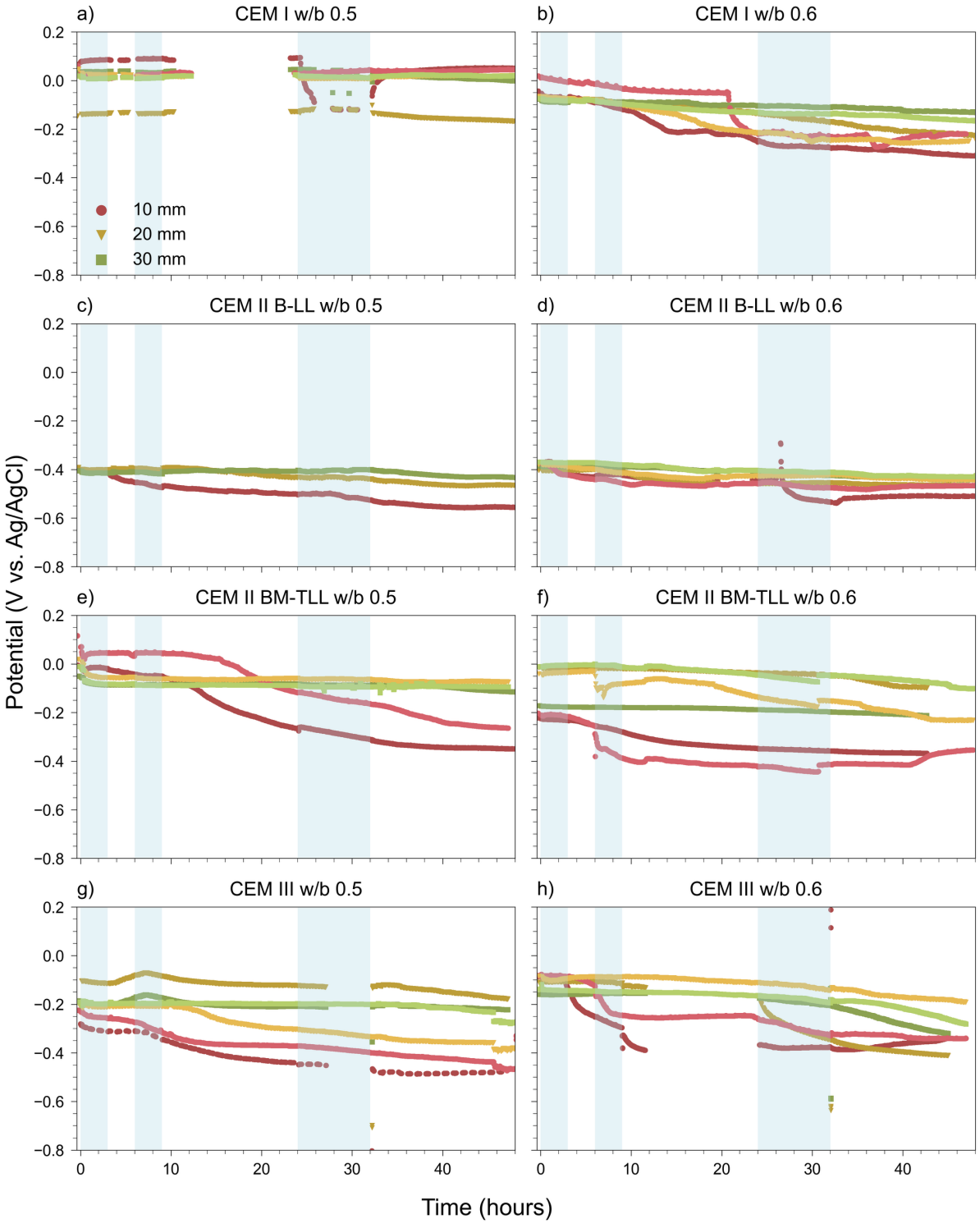

Figure 24 - Corrosion potential (V vs. Ag/AgCl) during the wet-dry cycles.

A.2 Review of moisture properties determination methods

Determination of moisture state and transport properties of carbonated cementitious materials: a review and recommended approaches

Introduction

Moisture related durability problems

Moisture is vital to concrete durability because it directly impacts the resistance to various forms of environmental and physical degradations. For instance, water evaporation can increase the risk of cracking and drying shrinkage. When concrete serves in aggressive environments, the harmful substances such as chlorides and sulfates can transport with liquid water which further cause corrosion of embedded steel reinforcement and other forms of chemical attack. Another main cause of steel corrosion is concrete carbonation which lowers the pH of concrete and thus weakens the ability to protect reinforcing steel bars. Laboratory experiments as well as practical experience show that steel corrosion in carbonated concrete occurs at a negligible rate as long as the moisture content in the concrete is below a certain threshold [1–3]. The two previous Cemsuisse research projects by ETH Zurich (no. 201807[1] and no. 202004[2]) also showed the similar results for different types of cementitious binders. This leads to the fact that *moisture content in carbonated concrete can be used to assess the risk of steel corrosion*, rather than only by the carbonation depth. Therefore, measuring and predicting moisture content is essential to understand if concrete remains durable, resilient, and capable of withstanding various environmental and mechanical stresses over its service life.

Moisture states

Water in concrete is from two sources, the leftover water for cement hydration reactions and external water from the environment when concrete is exposed to the high relative humidity (RH) environment. Movable moisture that can be involved in the transport process stays in pores, so the pore size and the pore network of the material are important. Owing to the complex structure and connectivity of the network, pores are in different shapes and randomly distribute which makes the quantification of the exact pores size distribution (PSD) extremely difficult. By assuming pores as cylinders, techniques can be used to measure PSD. Based on measurements using such as Scanning Electron Microscopy, Optical Microscopy, Impedance Spectroscopy and Mercury Intrusion Porosimetry (MIP), movable moisture in the pores in cementitious materials can be classified into different levels (see Table 11). Below interlayer water, there is some chemically bound water which is not concerned by moisture transport. Only in extreme conditions, this kind of water can be lost, such as drying at high temperature (e.g., 105 ºC).

[1] Projec title: „Sicherstellung der Dauerhaftigkeit von Stahlbetonbauten bei Karbonatisierung“
[2] Project title: „Sicherstellung der Dauerhaftigkeit von Stahlbetonbauten bei Karbonatisierung und wechselnder Nass/Trocken Exposition"

Table 11 Classification of pores and features in concrete (after [4])

Type of pore	Description	Size	Water	Properties
Capillary pores	Large	10 μm - 50 nm	Evaporable Bulk water	Permeability, strength
	Medium	50 -10 nm	Evaporable Moderate menisci	Permeability, strength, shrinkage (high RH)
Gel pores	Small	10 - 2.5 nm	Evaporable Strong menisci	Shrinkage (up to 50% RH)
	Micro	2.5 - 0.5 nm	Non-evaporable, no-menisci, inter-molecular interactions	Shrinkage, creep (35-11% RH)
Interlayer spaces	Structural	$<$ 0.5 nm	Non-evaporable, ionic/covalent bond	Shrinkage, creep ($<$11% RH)

Moisture transport mechanisms

Moisture transport in cementitious materials is related to many complex mechanisms which occur more or less jointly. In porous materials, several phenomena such as permeation, diffusion, adsorption-desorption-condensation and evaporation are very important [5]. They depend on the internal RH prevailing in the material.

Capillary transport

Capillary transport is the movement of liquid-water under the gradient of capillary pressure in porous media when there is no external hydraulic pressure. This is the result of interactions between liquid-water and pore walls. Capillary transport generally occurs when the liquid body is continuous. For high water content, the pores are almost filled with liquid-water. When a driving force is available, capillary flow is established through the liquid body in the porous network.

Water vapor diffusion

Ordinary diffusion is commonly found in both low RH and high RH ranges. It is caused by the gradient of vapor concentration, so water molecules tend to diffuse from the high concentration region to the low concentration zone. There are two main effects which can slow down ordinary diffusion. One is collisions between water molecules, which are able to offset some molecular momentum. The other one is the molecules exchange with adsorbed layer on pore walls. Water molecules adsorbed by pore walls decrease the ordinary diffusion process. When RH exceeds a threshold value, a meniscus is formed at each end of the path. In this condition, moisture transport becomes a process of condensation and evaporation at menisci. This mechanism is dominant in pores with size between 50 nm and 10 µm which is typically the size of capillary pores in cementitious materials (see Table 11).

Knudsen diffusion

According to the definition, Knudsen diffusion occurs if the pore size is the same as or smaller than the mean free path of the water molecules. This diffusion is governed by collisions against the pore walls, which are the main source of resistance to Knudsen diffusion. Knudsen diffusion can be quantified by the Knudsen number $Kn = \lambda/2r_p \geq 1$ where λ is the mean free path. For Knudsen diffusion, the value of Kn is equal to or greater than 1. The given free path in air at atmospheric pressure and room temperature (for instance 23 ºC) is around 68 nm. Hence,

Knudsen diffusion widely exists in gel pores and partially in capillary pores according to Table 11.

Surface film diffusion

This mechanism primarily takes place if water molecules are mainly adsorbed by pore walls (which is the case of low RH). On the one hand, when water molecules are forced toward the solid walls, they have the trend to be adsorbed by walls; on the other hand, due to the strong difference of molecules concentration at different distances from the pore walls, water molecules have another trend to leave the solid walls and to diffuse to lower concentration region. The result is that water molecules move near pore walls. It is governed by leaps of water molecules between different adsorption sites.

Evaporation-Condensation

Evaporation-Condensation occurs at the interface between liquid-water and gas. Moisture evaporates from the liquid surface and becomes vapor, so it can be transported by diffusion through the empty pore and condenses on the liquid surface at the other end of the pore. This process is due to the non-equilibrium between vapor pressure and capillary pressure in the vicinity of the interfaces.

Determination of moisture transport properties

In terms of transport efficiency (the mass of water), capillary transport of liquid water plays a significant role at the high RH and water vapor diffusion contributes more at the low RH [6]. At ETH Zurich, two previous Cemsuisse projects have focused on the effects of environmental conditions on steel corrosion in carbonated reinforced concrete. Four binders (CEM I, CEM II/B-LL, CEM II B/-M, CEM III/B), and two water-to-binder (w/b) ratios (0.5 and 0.6) were investigated. The investigated environmental factors include the humidity conditions (95% RH, 99% RH and WET, that is, in contact with liquid water). The project made a final conclusion that *only at the WET condition the measured corrosion rates seem significant*. This conclusion was also confirmed in other studies [1,3]. Therefore, the key moisture transport properties that should be investigated in the proposed project is liquid transport coefficients (e.g., liquid permeability, sorptivity, etc).

The commonly used methods to determine water absorption properties (sorptivity and water absorption coefficient) and water permeability are summarized in Figure 25. We will briefly introduce these methods and conclude the most feasible methods that can be used to determine moisture transport properties in a laboratory on the routine basis.

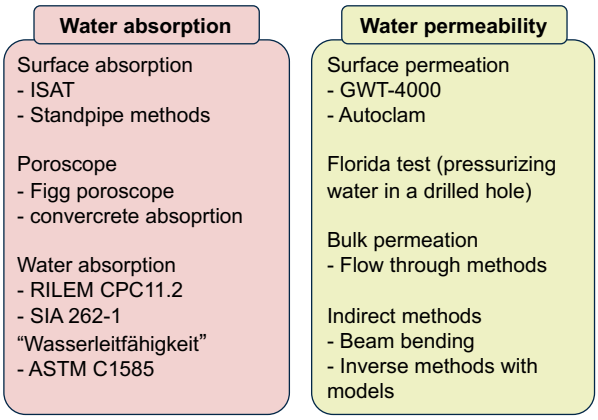

Figure 25 Moisture transport property measurements

Sorptivity and water absorption coefficient

For the hardened concrete, the sorptivity can be measured by various techniques (summarized in [7]), including Initial surface-absorption test, Figg water-absorption test, Covercrete-absorption test, Surface sorptivity test, etc. They all involve putting water with a certain height on the concrete surface or at several cm depth (by drilling a hole) and then reading the change of water head. These methods are not complicated to use, but the results are influenced by the initial moisture content and they are hard to achieve unidirectional water ingress. In the case of core drilling samples and carrying out water absorption tests in the laboratory, the above two problems can be easily solved.

Initial Surface Absorption Test (ISAT)

A simple method to test sorptivity on site is to use a reservoir filled with water and connect it to the concrete through a cap with known area [8]. The water reservoir should be placed in a way that the level of water in the reservoir is 200 ± 5 mm above the concrete surface. The water level in the reservoir is monitored by the sensor placed at the side of the reservoir and the data is sent to the computer through an A/D (analog-to-digital) converter. Before the start of the measurement, a calibration should be made, which converts vertical movement of the water level in the reservoir to the volume of water outflow from the reservoir. The outflow from the reservoir is equal to the water inflow into the concrete. The initial surface absorption value is then calculated.

Poroscope methods

The test is performed by drilling a hole perpendicular to the test surface with the hole dimensions. The hole is then cleared and rendered airtight using a rubber silicone plug that forms a cylindrical chamber. Once the rubber hardens, a typical syringe needle is pierced through the rubber and is applied with a certain water pressure. The chamber along with the attached capillary tube are then filled with water using the syringe. After 1 min (from the initial contact of water to concrete surface), the stopcock is shut, and the rate of water suction is observed by monitoring the meniscus movement in the horizontal capillary on the side. The time taken for the test concrete surface to absorb water is noted and reported as the test result.

RILEM CPC11.2

A cross-section surface of a concrete specimen with the height at least twice as large as the edge or diameter, resting on stable supports inside a recipient under atmospheric pressure, is submerged in water with a constant level of about 5 mm above the bottom surface of the specimen [9]. The specimen is covered with an enveloping vessel to avoid rapid evaporation of the water from the specimen (see Figure 26a). At different time intervals, the specimen is removed from water and the exposure surface is dried with the moist tissue (or cloth), and then the specimen mass is measured. By plotting water absorption against time, the slope of the curve (water absorption coefficient or sorptivity) can be determined (see Figure 26b).

ASTM C1585

The procedure for performing the water absorption test according to the ASTM standard [10] is similar to that recommended by RILEM. In this standard, the preconditioning of the specimens is recognized as the prevailing step as well. Specimens need to be in the environmental chamber at a temperature of 50 ± 2 °C and a RH of 80 ± 3% for 3 days. Subsequently, specimens should be placed inside a sealable container with free flow of air around the specimen. The container should be stored at 23 ± 2°C for at least 15 days before the start of the absorption procedure. This preconditioning ensures the equilibration of the moisture distribution within the test specimens and has been found to provide an internal RH of 50 to 70%, which is similar to RH found near the surface in some field structures.

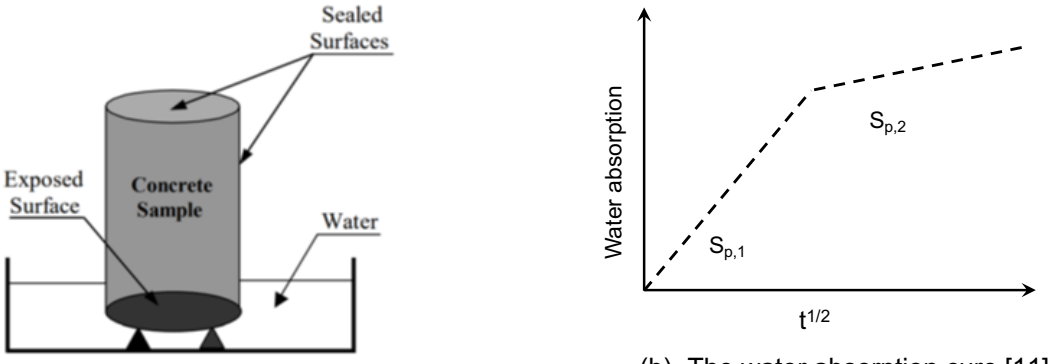

(a) Experiment setup

(b) The water absorption cure [11]

Figure 26 Illustration of water absorption test

An important (unsolved) question is which initial condition (RH) is appropriate to be used to determine moisture transport property. The standard ASTM C1585 suggests preconditioning specimens at 80% RH [10], while other studies showed that the initial RH can significantly affect the measured sorptivity [12]. In addition, depending on the specimen size, the precondition may take a very long time. Therefore, oven drying at the moderate temperature (e.g., 65 ºC) was commonly used in many studies [13,14].

Water permeability

Water permeability can be tested on-site with non-invasive methods, or in the laboratory on specimens taken from the structure or prepared in the laboratory. Instruments for testing water permeability on-site usually consist of a reservoir filled with water, which is connected to the concrete surface, a syringe or vacuum pump for introducing pressure into the reservoir and a transducer for monitoring pressure. Most of the laboratory methods consist of placing the

concrete specimen under a pressurized water flow and measuring the amount of water penetrated through the concrete.

Surface permeation

The surface permeation of liquid water can be measured by the Germann test and an Autoclam device. The Germann water permeability test is used for on-site evaluation of the water permeation of the skin-concrete in finished structure. In this method, a pressure chamber containing a watertight gasket is secured and held tightly against the test surface. The chamber is then filled with water and the values are shut. The selected pressure is maintained using a micrometer gage pressing a piston into the water-filled chamber. The piston travel with time is used to characterize the permeation property of the test surface. The testing procedure is partially destructive in nature and therefore requires repair of the holes after testing. The Autoclam method uses a similar principle but with a different design for the device. The test procedure includes pumping the water to the test region via a priming pump, and the pressure of water is measured using a pressure transducer. Once the testing chamber is filled with water, the priming pump turns off automatically. At the applied pressure, water transport that takes place in the capillary pores does not occur from the pressure induced flow, but instead from the absorption. As the water absorption proceeds, the pressure tends to decline and is maintained constantly via a pump with a control system. The volume of water is measured with time, so the surface water absorption can be determined. The test method is nondestructive in nature and could be used both for lab and on-site specimens.

Florida test

The Florida test measures water penetration through a drilled hole into concrete. The drilled hold is about 152 mm in depth and a cylindrical probe is introduced into the hole. The top nut is then tightened to seal the central chamber. The chamber is then applied with a full vacuum after which the probe is connected to the instrument unit. Using nitrogen, water is then pressurized into the chamber via the probe, which then flows into the surrounding concrete. Once a steady flow is attained, the water flow rate is recorded (with a mean value of five measurements) and the water permeability coefficient is calculated in accordance with Darcy's law [15].

Bulk permeation (Flow through methods)

Conventional methods to measure water permeability are classified as flow-through techniques, as they measure the flux under steady state conditions for fully saturated specimens, with the geometry of either truncated cones [16] or cylinders/disks [17–22]. During measurements, liquid water is pressurized at one face and the outflow at the opposite face is continuously measured until the flow reaches a steady state, and then water permeability can be calculated by using Darcy's law. In these methods, it may take a long time to reach steady state flow (e.g., several weeks) for low permeable materials. To reduce the measurement time, it was suggested to increase the applied pressure [21], but this may risk altering the microstructure of materials and increasing the water leak at the interface between the specimen and the pressure cell. Instead of applying continuous constant pressure, pressure relaxation methods involve increasing pressure on one side and observing the decrease of pressure due to liquid being pushed to another side (e.g., [23]). Applying a constant water flow was also used in some studies (e.g., [20]). These methods are rapid, but they still need high pressure and thus have the same problems as the other conventional flow-through methods.

Recent studies used hollow cylinders [24] which measured radial flow of water under applied pressure. The main advantage of this kind of method is that the total area through which fluids flow is much larger than the disc specimens; therefore, the measurements showed higher accuracy and repeatability [24,25]. On the other hand, the large area increases the risk of heterogeneity, which means that any cracks or areas having greater water flow can significantly change the results.

Indirect methods

Indirect methods, requiring the other data to calculate, are called poromechanical (dynamic pressurization) techniques which monitor the time-dependent deformation of a specimen induced by externally applied stress or temperature change. The dynamic pressurization (DP) is one of such methods, which keeps the specimen in a sealed vessel and suddenly increasing or decreasing the pressure [26,27]. The hollow cylinders were also used in the DP method to improve the measurement accuracy [25,28]. By alternatively pressurizing and depressurizing, the effect of air voids in the unsaturated specimen can be gradually removed [27]. The beam-bending (BB) method is another example [29,30]. The measured relaxation curve that is obtained when a certain strain is applied to a long and slender specimen includes both hydrodynamic and viscoelastic effects. Therefore, permeability can be determined by fitting the relaxation curve with a theoretical model. The deformation of a specimen can also be introduced by the thermal expansion [31–33], in which the rate of thermal strain relaxation is used to determine because the liquid shows a greater expansion than the solid phase.

Water permeability measurements are very sensitive to saturation conditions since the fully saturated condition is not easy to achieve. The presence of air voids or entrapped air in non-fully saturated materials may have a great influence on the measured results of the poromechanical methods and cause long delays in reaching equilibrium in conventional methods [34]. To ensure the fully saturated condition, various approaches were used in the literature, such as curing the specimen in water/limewater [22,24], vacuum saturation and pressurizing saturation [29,30]. The time needed to fully saturate a porous body increases with the square of its smallest dimension. For the direct methods, the thickness of a disc specimen ranges from 25 to 70 mm (see the review in [21]) depending the size of aggregates as El-Dieb and Hooton [17] suggested that the specimen thickness should be 3 times as large as the aggregate size and a recent study [35] even reported that the specimen needs to be about 10 times as thick as the aggregates; therefore, a specimen may be extremely difficult to saturate.

Inverse analysis

Our previous study introduced two methods to indirectly determine water permeability [36]. One is called “inverse analysis” that utilizes a numerical moisture transport model to back-calculate based on a measured drying mass loss curve or wetting mass increasing curve. The other one employs the measured diffusivity curve to fit by a general expression including both liquid transport and vapor diffusion. One factor that may affect the results of theoretical models is the diffusion of water vapor, as this phase is neglected in some models, but our studies show that the neglect can underestimate mass transport at low RHs [36].

Determination of moisture content

There exist various methods measuring the moisture state in concrete, as summarized in Figure 27. The State-of-the-Art Report of the RILEM TC 248-MMB summarized the common techniques that can determine moisture content in building materials [37], including nuclear

magnetic resonance (NMR), X-ray attenuation, Gamma-ray attenuation, Neutron Radiography, Microwave Reflection, Capacimetry, Time Domain Reflectometry, etc. The first four methods are based on the electric or magnetic properties of molecules or atoms. They are able to in principle provide measured data with high resolution in 1D profiles or 2D maps. The last three measure RH or electrical resistivity of the porous material, which provide the bulk information with a coarse resolution. All these methods only provide signals reflecting moisture variations and need calibration data to determine moisture content.

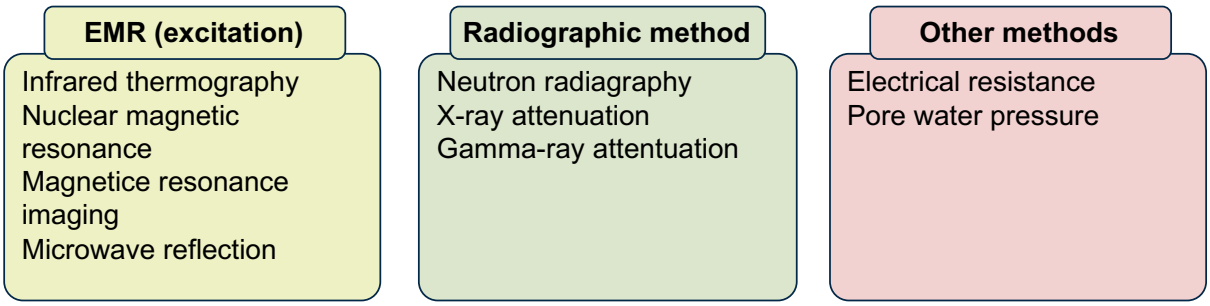

Figure 27 Methods of determining moisture state in concrete. EMR= electromagnetic radiation.

Infrared thermography

The infrared thermography, a non-contact technique, is a non-destructive technique allowing the evaluation of the material surface temperature. The method records the electro-magnetic ray in the infrared spectrum, emitted from the external surface. The surface temperature of a material is influenced by the moisture conditions in some cases; this could be detected by IR-thermography. Thermal radiations are the function of a material's internal properties (composition, moisture content, and possible damage) and external conditions (sunlight, heat sources, rains). The infrared thermography allows assessing the luminance, which can be translated in terms of surface temperature, through the radiometric equation. The principle is then to assess the effect resulting on the surface of the material's internal characteristics (for our case, moisture content), influenced by the surrounding conditions. Measurement is generally done with a numeric thermal camera that records the 2D thermal field on the investigated surface. The interpretation is essentially qualitative aiming at regions with large moisture variations. Clearly, this technique only works for the material surface.

Nuclear magnetic resonance

Nuclear magnetic resonance (NMR) is a non-destructive technique that enables the depth-resolved determination of the water content inside a sample. It is versatile and can be adjusted to the demands of an experiment. NMR can be used to measure the hydrogen nuclei contained in porous media, based on the interaction of the magnetic dipole moment of a nuclei spin with an outer magnetic field. The orientation of the magnetic moments is manipulated by electromagnetic radio pulses at certain frequencies. Depending on the number of peaks of the NMR signals, it can detect water in different ranges of pores [38,39].

Radiographic methods

A radiographic method is in general based on the universal law of attenuation of radiation transmitted through the tested material. Since the transmission/absorption differs for different compositions and thickness, the information on the structure and composition of the tested

materials can be obtained by radiographic measurement. For cementitious materials, both electromagnetic radiation (X-rays and gamma rays) and particle radiation (neutron) are used to determine the water distribution. Although X-rays may be sufficient for certain materials, the direct measurement of moisture content within concrete is particularly difficult because of the high initial density of the material, low density changes caused by moisture transport, variability in performance of the X-ray scanning equipment over time, and the varying X-ray scattering artefacts caused by changing water conditions in a highly heterogeneous material structure [40]. To overcome these problems, studies have introduced contrast agents (e.g., CsCl) into water to improve contrast [41,42]. However, these ions would change the chemical composition of pore solution and be absorbed on solids becoming immobile in the pore network. Gamma rays detect the changes of material's density, so by assuming that only moisture transport causes the changes, moisture variations can be measured [43]. Neutrons are more sensitive to water than other radiations, so neutron radiography is often used to detect water movement in cementitious materials [44,45] and the effect of steel bars [3].

Electrical resistance

Electrical resistance is the ability for a porous material to impede the flow of electrical current. The resistance is a function of the geometry of the tested body and measurement device. So, the resistivity is generally expressed in ohm·meter, representing the intrinsic material's property. Because the electrical resistivity of a porous material changes with its moisture content, by measuring the changes of resistivity, the moisture transport process can be reflected [46].

Mathematic models

To determine moisture content at a certain depth, an alternative way is to use a moisture transport model, which can simulate the process of moisture moving inside concrete. Theoretically, moisture content at any depths and any locations can be determined by model simulations with a flexible resolution. For most models in the literature, such as the continuum one-phase, two-phase and multi-phase models [5], the key parameter controlling moisture transport is the moisture transport coefficient, which shows how fast moisture can move inside a porous medium. There are different types of coefficients to quantify the transport velocity, such as moisture diffusivity, liquid water permeability (see Section 0), and sorptivity (or rate of water absorption, see Section 0). After knowing the transport coefficient, plus the initial and boundary conditions, the moisture distribution in a porous material can be simulated by the moisture transport model.

Water vapor sorption isotherms

At equilibrium state, moisture content can be indirectly calculated by RH in the surrounding environment. The relation between RH and moisture content is known as the material's water retention curve (for soils and other more porous materials) or water vapor sorption isotherms (for low permeable materials). Even though moisture transport in a porous material is a dynamic process, for the low permeable materials like concrete, the assumption of the quasi-equilibrium between RH and moisture content is valid [47]. Therefore, for a given cementitious material, by measuring the water vapor sorption isotherm, the corresponding moisture content at different RHs can be determined. In addition, the sorption isotherms are also needed for the most moisture transport models as the input data.

The sorption isotherms can be measured by either the saturated salt solution method (SSS) or a dynamic vapor sorption analyzer (DVS) [48]. They both keep a piece of material under a certain RH until its mass reaches equilibrium. The main difference between two methods is the

samples size as a DVS can only measure very small sample (less than 1 g) so aggregates and sands need to be removed. Measurements only quantify the sorption behavior for the paste in concrete or mortar, rather than the global sorption behavior of concrete [5]. However, if comparing moisture content in cement paste (from concrete or separately prepared cement paste) with concrete with the same w/c and cement, their sorption isotherms agree well in the low and moderate humidity range [49].

Recommendations

Different techniques that can determine moisture transport properties, moisture content and moisture state have been reviewed. To select the most feasible ones for the proposed project, the following facts need to be considered.

1) Liquid water at high RH or near-saturation conditions is more interesting to us than water vapor in cementitious materials. As already concluded in the literature [1–3], serious corrosion in carbonated concrete is only found at the high moisture content or when concrete is directly in contact with liquid water. Therefore, we should mainly focus on moisture transport under these conditions. Furthermore, considering the efficiency of moisture transport by the mass of different phases, liquid water transport is much higher than water vapor because of the higher density of liquid water [50]. Therefore, the measurements of capillary water absorption and liquid water permeability are the most relevant methods.
2) The measured moisture properties need to represent the bulk concrete. This means that tests that can only measure the surface moisture are not sufficient. The tests use small samples or cement paste should be excluded in the proposed project.
3) The selected methods should be more practical for a normal lab and can be carried out as the routine tests (called "*simple moisture test methods*" in the proposal). Therefore, the radiographic techniques may not be suitable for most laboratory requirements.
4) The measured short-term laboratory data need to be extended to the long term and applied to different moisture conditions (imagining the service conditions of concrete structures). The laboratory tests can only be carried out under the given experimental conditions. To fulfill this requirement, a moisture transport model is needed to simulate moisture transport and further to predict the service life of the concrete structure under various environmental conditions.

Based on the above considerations, water absorption tests are needed to study water transport when a concrete structural element is in direct contact with liquid water. The flow through methods are the first choice to measure liquid permeability as they are straightforward and use large concrete samples unlike some indirect methods that can only measure permeability of small samples (e.g., the beam bending method). However, the sealing problem and potential damages still need to be solved for the flow through methods. Alternatively, the inverse analysis method can be selected if the flow through methods are not available. It can use the same moisture transport model as the fourth point of the above facts for the long-term moisture transport prediction. Another advantage of using inverse analysis is able to reduce the number of tests.

According to the concluded methods to determine moisture state and transport properties of carbonated cementitious materials, we propose the conceptual approach for assessing steel corrosion as shown in Figure 28. An established moisture transport model will be used to complement the moisture transport experiments and thus to provide broader support for the

suggested approach. Such a model-based approach is needed to predict the long-term service life of concrete structures in particular for these already carbonated.

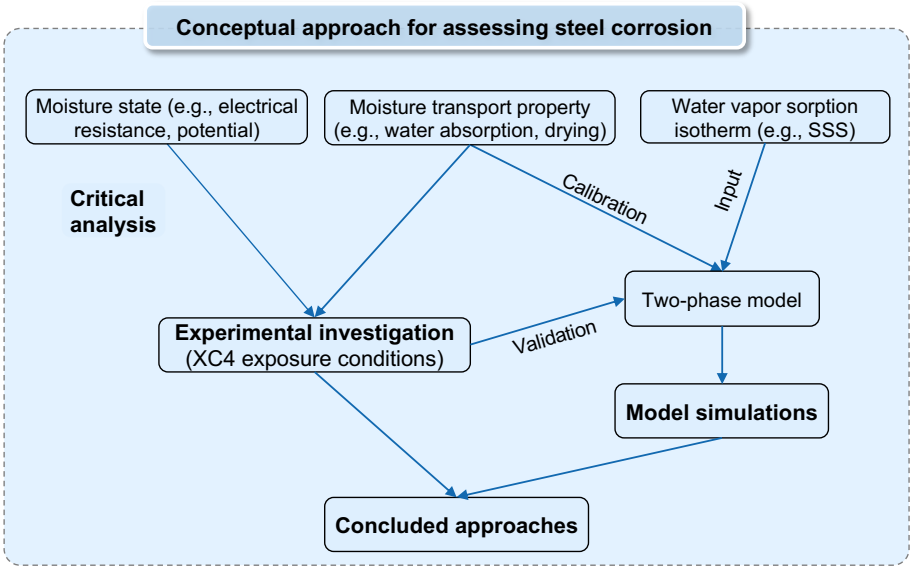

Figure 28 The work flow of the proposed project to develop a new conceptual approach to assess steel corrosion in carbonated concrete.

References

[1] C. Alonso, C. Andrade, J.A. González, Relation between resistivity and corrosion rate of reinforcements in carbonated mortar made with several cement types, Cem Concr Res 18 (1988) 687–698. https://doi.org/10.1016/0008-8846(88)90091-9.

[2] M. Stefanoni, U.M. Angst, B. Elsener, Electrochemistry and capillary condensation theory reveal the mechanism of corrosion in dense porous media, Sci Rep 8 (2018) 1–10. https://doi.org/10.1038/s41598-018-25794-x.

[3] Z. Zhang, P. Trtik, F. Ren, T. Schmid, C.H. Dreimol, U. Angst, Dynamic effect of water penetration on steel corrosion in carbonated mortar: A neutron imaging, electrochemical, and modeling study, Cement 9 (2022) 100043. https://doi.org/10.1016/j.cement.2022.100043.

[4] S. Mindess, J.F. Young, D. Darwin, Concrete, Prentice-Hall, Englewood Cliffs, N.J., 2003.

[5] Z. Zhang, Modelling of Sorption Hysteresis and Its Effect on Moisture Transport Within Cementitious Materials, Ph.D. thesis, Universite Paris-Est, 2014. https://doi.org/10.13140/RG.2.1.1918.8082.

[6] Z. Zhang, G.W. Scherer, Determination of water permeability for a moisture transport model with minimized batch effect, Constr Build Mater 191 (2018) 193–205. https://doi.org/10.1016/j.conbuildmat.2018.09.194.

[7] ACI 228.2R, Report on nondestructive test methods for evaluation of concrete in structures, 2013.

[8] A.E. Long, G.D. Henderson, F.R. Montgomery, Why assess the properties of near-surface concrete?, Constr Build Mater 15 (2001) 65–79. https://doi.org/10.1016/S0950-0618(00)00056-8.

[9] H. Beushausen, L. Fernandez Luco, Performance-Based Specifications and Control of Concrete Durability: State-of-the-Art Report RILEM TC 230-PSC, Performance-Based Specifications and Control of Concrete Durability: State-of-the-Art Report RILEM TC 230-PSC 18 (2015) 1–373. https://doi.org/10.1007/978-94-017-7309-6.

[10] ASTM C1585-20, Standard Test Method for Measurement of Rate of Absorption of Water by Hydraulic Cement Concretes, ASTM International (2020) 1–6. https://doi.org/10.1520/C1585-13.2.

[11] Z. Zhang, U. Angst, A Dual-Permeability Approach to Study Anomalous Moisture Transport Properties of Cement-Based Materials, Transp Porous Media 135 (2020) 59–78. https://doi.org/10.1007/s11242-020-01469-y.

[12] J. Castro, D. Bentz, J. Weiss, Effect of sample conditioning on the water absorption of concrete, Cem Concr Compos 33 (2011) 805–813. https://doi.org/10.1016/j.cemconcomp.2011.05.007.

[13] Z. Zhang, U. Angst, Microstructure and moisture transport in carbonated cement-based materials incorporating cellulose nanofibrils, Cem Concr Res 162 (2022) 106990. https://doi.org/10.1016/j.cemconres.2022.106990.

[14] F. Ren, C. Zhou, Q. Zeng, Z. Zhang, U. Angst, W. Wang, Quantifying the anomalous water absorption behavior of cement mortar in view of its physical sensitivity to water, Cem Concr Res 143 (2021) 106395. https://doi.org/10.1016/j.cemconres.2021.106395.

[15] J. Milla, T.L. Cavalline, T.D. Rupnow, B. Melugiri-Shankaramurthy, G. Lomboy, K. Wang, Methods of test for concrete permeability: A critical review, 2021. https://doi.org/10.1520/ACEM20200067.

[16] B.K. Nyame, J.M. Illston, Relationships between permeability and pore structure of hardened cement paste, Magazine of Concrete Research 33 (1981) 139–146. https://doi.org/10.1680/macr.1981.33.116.139.

[17] A.S. El-Dieb, R.D. Hooton, Water-permeability measurement of high performance concrete using a high-pressure triaxial cell, Cem Concr Res 25 (1995) 1199–1208. https://doi.org/10.1016/0008-8846(95)00112-P.

[18] L. Bágel', V. Živica, Relationship Between Pore Structre and Permeability of Hardened Cement Mortars: on the Choice of Effective Pore Structure Parameter, Cem Concr Res 27 (1997) 1225–1235. https://doi.org/10.1016/S0008-8846(97)00111-7.

[19] G. Ye, Percolation of capillary pores in hardening cement pastes, Cem Concr Res 35 (2005) 167–176. https://doi.org/10.1016/j.cemconres.2004.07.033.

[20] Q.T. Phung, N. Maes, G. De Schutter, D. Jacques, G. Ye, Determination of water permeability of cementitious materials using a controlled constant flow method, Constr Build Mater 47 (2013) 1488–1496. https://doi.org/10.1016/j.conbuildmat.2013.06.074.

[21] Z.A. Kameche, F. Ghomari, M. Choinska, A. Khelidj, Assessment of liquid water and gas permeabilities of partially saturated ordinary concrete, Constr Build Mater 65 (2014) 551–565. https://doi.org/10.1016/j.conbuildmat.2014.04.137.

[22] C. Zhou, W. Chen, W. Wang, F. Skoczylas, Indirect assessment of hydraulic diffusivity and permeability for unsaturated cement-based material from sorptivity, Cem Concr Res 82 (2016) 117–129. https://doi.org/10.1016/j.cemconres.2016.01.002.

[23] W. Brace, J. Walsh, W.F.-J. of Geophysical, undefined 1968, Permeability of granite under high pressure, Wiley Online LibraryWF Brace, JB Walsh, WT FrangosJournal of Geophysical Research, 1968•Wiley Online Library 73 (1968) 2225–2236. https://doi.org/10.1029/JB073i006p02225.

[24] A. Amriou, M. Bencheikh, New experimental method for evaluating the water permeability of concrete by a lateral flow procedure on a hollow cylindrical test piece, Constr Build Mater 151 (2017) 642–649. https://doi.org/10.1016/j.conbuildmat.2017.06.126.

[25] C.A. Jones, Z.C. Grasley, Correlation of radial flow-through and hollow cylinder dynamic pressurization test for measuring permeability, Journal of Materials in Civil Engineering 21 (2009) 594–600. https://doi.org/10.1061/(ASCE)0899-1561(2009)21:10(594).

[26] G.W. Scherer, Dynamic pressurization method for measuring permeability and modulus: I. Theory, Materials and Structures/Materiaux et Constructions 39 (2006) 1041–1057. https://doi.org/10.1617/S11527-006-9202-0.

[27] Z.C. Grasley, G.W. Scherer, D.A. Lange, J.J. Valenza, Dynamic pressurization method for measuring permeability and modulus: II. cementitious materials, Materials and Structures/Materiaux et Constructions 40 (2007) 711–721. https://doi.org/10.1617/s11527-006-9184-y.

[28] J.L. Rose, Z.C. Grasley, Comparison of Permeability of Cementitious Materials Obtained via Poromechanical and Conventional Experiments, Journal of Materials in Civil Engineering 29 (2017) 04017083. https://doi.org/10.1061/(asce)mt.1943-5533.0001931.

[29] W. Vichit-Vadakan, G.W. Scherer, Measuring permeability of rigid materials by a beam-bending method: III, cement paste, Journal of the American Ceramic Society 85 (2002) 1537–1544. https://doi.org/10.1111/j.1151-2916.2002.tb00309.x.

[30] W. Vichit-Vadakan, G.W. Scherer, Measuring permeability and stress relaxation of young cement paste by beam bending, Cem Concr Res 33 (2003) 1925–1932. https://doi.org/10.1016/S0008-8846(03)00168-6.

[31] G.W. Scherer, Measuring permeability by the thermal expansion method for rigid or highly permeable gels, J Solgel Sci Technol 3 (1994) 31–40. https://doi.org/10.1007/BF00490146.

[32] G.W. Scherer, Thermal Expansion Kinetics: Method to Measure Permeability of Cementitious Materials: I, Theory, Journal of the American Ceramic Society 83 (2004) 2753–2761. https://doi.org/10.1111/j.1151-2916.2000.tb01627.x.

[33] H. Ai, J.F. Young, G.W. Scherer, Thermal Expansion Kinetics: Method to Measure Permeability of Cementitious Materials: II, Application to Hardened Cement Pastes, Journal of the American Ceramic Society 84 (2004) 385–91. https://doi.org/10.1111/j.1151-2916.2001.tb00666.x.

[34] G.W. Scherer, Poromechanics analysis of a flow-through permeameter with entrapped air, Cem Concr Res 38 (2008) 368–378. https://doi.org/10.1016/j.cemconres.2007.09.028.

[35] Z. Wu, H.S. Wong, N.R. Buenfeld, Influence of drying-induced microcracking and related size effects on mass transport properties of concrete, Cem Concr Res 68 (2015) 35–48. https://doi.org/10.1016/j.cemconres.2014.10.018.

[36] Z. Zhang, M. Thiery, V. Baroghel-Bouny, Investigation of moisture transport properties of cementitious materials, Cem Concr Res 89 (2016) 257–268. https://doi.org/10.1016/j.cemconres.2016.08.013.

[37] L.O. Nilsson, Methods of measuring moisture in building materials and structures: State-of-the-art report of the rilem technical committee 248-mmb, in: RILEM State-of-the-Art Reports, 2018: pp. 1–280. https://doi.org/10.1007/978-3-319-74231-1.

[38] C. Zhou, F. Ren, Q. Zeng, L. Xiao, W. Wang, Pore-size resolved water vapor adsorption kinetics of white cement mortars as viewed from proton NMR relaxation, Cem Concr Res 105 (2018) 31–43. https://doi.org/10.1016/j.cemconres.2017.12.002.

[39] R.M.E. Valckenborg, NMR on technological porous materials, 2001.

[40] T. Oesch, F. Weise, D. Meinel, C. Gollwitzer, Quantitative In-situ Analysis of Water Transport in Concrete Completed Using X-ray Computed Tomography, Transp Porous Media 127 (2019) 371–389. https://doi.org/10.1007/s11242-018-1197-9.

[41] Q. Zeng, X. Wang, R. Yang, N. Jike, Y. Peng, J. Wang, Y. Tian, C. Zhou, S. Ruan, D. Yan, Transmission micro-focus X-ray radiographic measurements towards in-situ tracing capillary imbibition fronts and paths in ultra-thin concrete slices, Measurement (Lond) 175 (2021). https://doi.org/10.1016/j.measurement.2021.109141.

[42] L. Yang, Y. Zhang, Z. Liu, P. Zhao, C. Liu, In-situ tracking of water transport in cement paste using X-ray computed tomography combined with CsCl enhancing, Mater Lett 160 (2015) 381–383. https://doi.org/10.1016/J.MATLET.2015.08.011.

[43] G. Villain, M. Thiery, Gammadensimetry: A method to determine drying and carbonation profiles in concrete, NDT and E International 39 (2006) 328–337. https://doi.org/10.1016/j.ndteint.2005.10.002.

[44] P. Zhang, F.H. Wittmann, T. Zhao, E.H. Lehmann, Neutron imaging of water penetration into cracked steel reinforced concrete, Physica B Condens Matter 405 (2010) 1866–1871. https://doi.org/10.1016/j.physb.2010.01.065.

[45] N. Toropovs, F. Lo Monte, M. Wyrzykowski, B. Weber, G. Sahmenko, P. Vontobel, R. Felicetti, P. Lura, Real-time measurements of temperature, pressure and moisture profiles in High-Performance Concrete exposed to high temperatures during neutron radiography imaging, Cem Concr Res 68 (2015) 166–173. https://doi.org/10.1016/j.cemconres.2014.11.003.

[46] C.K. Larsen, Electrical resistivity of concrete - Part II: Influence of moisture content and temperature, (2006). https://doi.org/10.1617/2351580028.100.

[47] Z. Zhang, U.M. Angst, Effects of model boundary conditions on simulated drying kinetics and inversely determined liquid water permeability for cement-based materials, Drying Technology 40 (2022) 2741–2758. https://doi.org/10.1080/07373937.2021.1961800.

[48] P. Arlabosse, E. Rodier, J.H. Ferrasse, S. Chavez, D. Lecomte, E. Rodier, J.H. Ferrasse, S. Chavez, D. Lecomte, Comparison Between Static and Dynamic Methods for Sorption Isotherm Measurements Comparison Between Static and Dynamic Methods for Sorption, Drying Technology: An International Journal 3937 (2017) 479–497. https://doi.org/10.1081/DRT-120018458.

[49] V. Baroghel-Bouny, Water vapour sorption experiments on hardened cementitious materials. Part I: Essential tool for analysis of hygral behaviour and its relation to pore structure, Cem Concr Res 37 (2007) 414–437. https://doi.org/10.1016/j.cemconres.2006.11.019.

[50] Z. Zhang, M. Thiéry, V. Baroghel-Bouny, Analysis of moisture transport in cementitious materials and modelling of drying-wetting cycles, Proceedings of the International Conference on Numerical Modeling Strategies for Sustainable Concrete Structures (SSCS 2012) (2012) 1–11.